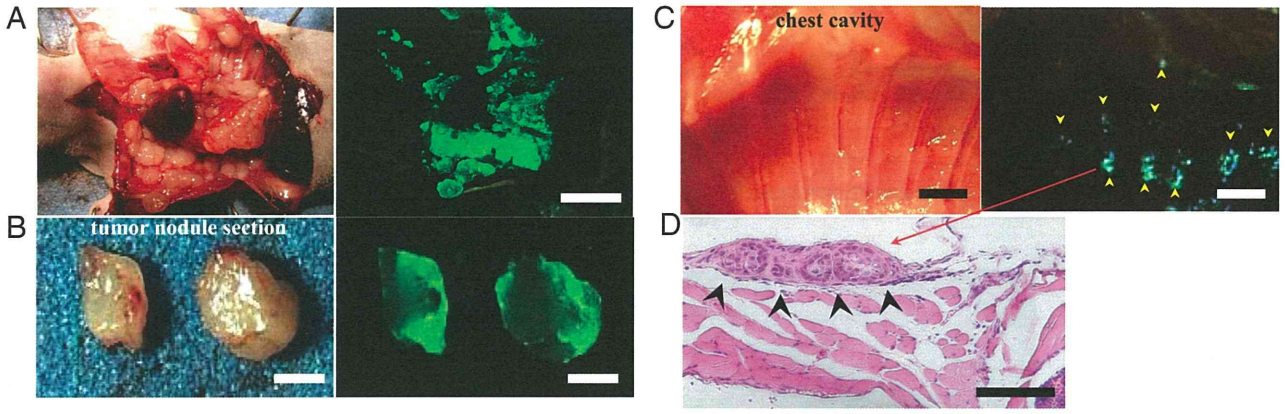

Fig. 4. Intrapleural injection of OBP-401 visualized pleural disseminations of A549 cells. (*A*) Two weeks after implantation of noncolored A549 cells into the thoracic space, OBP-401 at a dose of 1×10^8 PFU, was intrapleurally injected. Five days later, disseminated nodules were visualized by GFP fluorescence (*Right*). (Scale bar, 10 mm.) (*B*) Cross-section of pleural disseminated nodule. GFP expression was seen on the surface of pleurally disseminated nodules (*Right*). (Scale bar, 2 mm.) (*C*) Very small lesions that were not detectable in brightfield were visualized by GFP fluorescence (*Right*, arrowheads). (Scale bar, 2 mm.) (*D*) Histological analysis with H&E confirmed that these GFP-expressing lesions were adenocarcinomas (arrowheads). (Scale bar, 100 μm.)

was essentially coincident with that of GFP (Fig. 3*C*). These results indicate that i.p. injection of OBP-401 efficiently infected and labeled disseminated cancer.

Labeling of Pleurally Disseminated Cancer with OBP-401. These experiments assessed the effectiveness of OBP-401 labeling of pleural carcinomatosis in a mouse model of unlabeled A549 human lung cancer cells. The thoracic space of nude mice was inoculated with 2×10^6 cancer cells. Various sized disseminated plural nodules appeared within 10 days after implantation. At this time, 1×10^8 PFU of OBP-401 were injected into the thoracic cavity. Five days after injection of OBP-401, the cavity was examined using GFP fluorescence imaging. A representative mouse is shown in Fig. 4. Disseminated pleural nodules were visualized by GFP expression (Fig. 4 *A* and *B*). Even very small lesions, which are normally undetectable, were clearly illuminated by GFP fluorescence (Fig. 4*C*). Histological examination confirmed that these GFP-expressing tissues were adenocarcinomas. A representative histological section is shown in Fig. 4*D*. These results suggest that intrapleural injection of at least 1×10^8 PFU of OBP-401 can efficiently label disseminated pleural cancer. Lower doses of OBP-401 resulted in less efficient labeling.

OBP-401 Fluorescence-Guided Resection of Disseminated Peritoneal Tumors. In order to test the effectiveness of OBP-401-guided cytoreduction surgery, we used the peritoneal carcinomatosis model with nonfluorescent HCT-116 human colon cancer cells. Mice with peritoneal carcinomatosis were injected i.p. with OBP-401 at a dose of 1×10^8 PFU. Five days after viral administration, laparotomy was performed to remove intra-abdominal disease using fluorescence-guided navigation under anesthesia (Fig. 5 *A* and *B*). A representative mouse after cytoreduction surgery with OBP-401-navigation is shown in Fig. 5*C*. Disseminated cancer nodules, which would otherwise be undetectable, were clearly visible by bright GFP fluorescence. The resected nodules were visualized as frozen sections under both fluorescence (Fig. 5*D*) and after hematoxylin and eosin (H&E) staining (Fig. 5 *E* and *F*). These results suggest that OBP-401-labeling has significant potential for guiding cytoreduction surgery of disseminated cancer.

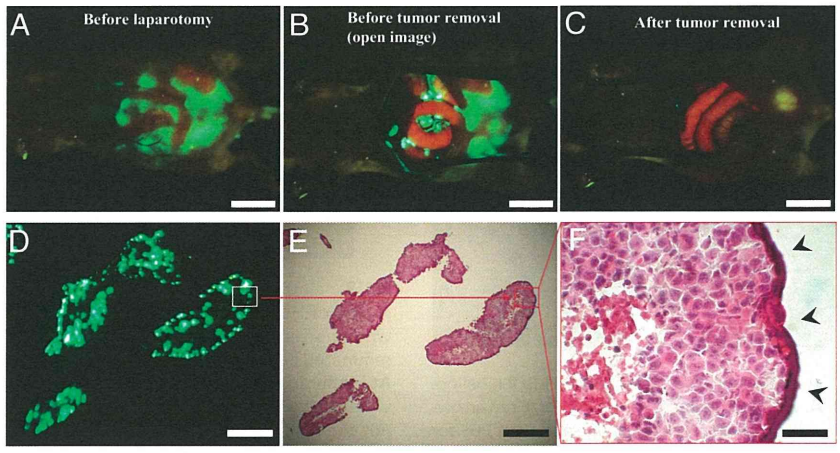

Fig. 5. Fluorescence-guided surgical removal of peritoneal disseminated HCT-116 tumors after GFP labeling with OBP-401. Noncolored HCT-116 human colon cancer cells were injected into the abdominal space of nude mice. Ten days later, 1×10^8 PFU of OBP-401 were i.p. injected. (*A*) Disseminated nodules were efficiently labeled and noninvasively visualized by GFP expression 5 days after virus administration. (*B*) Under general anesthesia, laparotomy was performed to remove intra-abdominal disease under GFP-guided navigation. (*C*) Disseminated nodules visualized by GFP-guided navigation were removed. (Scale bars: *A–C*, 10 mm.) (*D*) Frozen section of resected HCT-116 disseminated nodules with fluorescence detection. (Scale bar, 500 μm.) (*E*) H&E section of HCT-116 disseminated nodules shown in *D*. The box outlines a region of *D* and *E* analyzed in *F*. (Scale bar, 500 μm.) (*F*) Detail of the boxed region of *D* and *E*. (Scale bar, 50 μm.)

Discussion

The peritoneal surface is involved in more than 20% of patients with gastric, colon, and pancreatic cancers (1). Cytoreduction surgery requires resection of all visible tumors and stripping of all peritoneal surfaces that contain metastatic nodules (1, 2, 9). Therefore, visceral peritoneal involvement often requires concomitant resection of intra-abdominal organs such as the small intestine and colorectum.

The detection of small macroscopic peritoneal lesions is largely limited by the weak contrast between tumor nodules and surrounding normal tissues. Technology improving the intraoperative detection of peritoneal disease would facilitate essentially complete cytoreduction in these patients. The photosensitizer, 5-aminolevulinic acid (5-ALA) has been used for intraoperative detection of cancer lesions in neurosurgery (10). However, labeling that is essentially cancer-selective can be a powerful surgical adjunct. This report shows that OBP-401 infection of cancer cells leads to the highly selective induction of bright GFP fluorescence.

Implanting RFP-expressing cancer cell lines gave rise to fluorescent nodules whose color change clearly indicated the efficiency with which OBP-401 labeled disseminated peritoneal tumors with GFP. The change from red to yellow fluorescence indicated successful infection by OBP-401 (Fig. 3). Similarly, OBP-401 GFP labeling could detect dissemination nodules with high sensitivity in a pleural carcinomatosis model (Fig. 4).

Perhaps most importantly, we could remove disseminated disease in a peritoneal carcinomatosis model by using fluorescence-guided resection. These results suggest developing a dedicated excitation light for fluorescence-guided surgery similar to that described for use in mice (11). In the present study, during surgery, even very small peritoneal lesions could be identified with GFP fluorescence (11).

Materials and Methods

Recombinant Adenovirus. OBP-401, containing the *GFP* gene under the control of the CMV promoter with the hTERT promoter driving the *E1A* and *E1B* genes, was constructed as previously described (6, 7). OBP-401 was purified by ultracentrifugation in cesium chloride step gradients. Virus titers were determined by a plaque-forming assay using 293 cells. The virus was stored at −80°C.

Cell Culture. The human non-small cell lung cancer cell line A549, the human colorectal cancer cell lines HCT-116 and HT-29, and the human prostate cancer cell line PC-3 were cultured in RPMI 1640 medium supplemented with 10% FBS.

Production of RFP Retroviral Vector. For RFP retrovirus production, the *Hind*III/*Not*I fragment from pDsRed2 (Clontech), containing the full-length RFP cDNA, was inserted into the *Hind*III/*Not*I site of pLNCX2 (Clontech) containing the neomycin-resistance gene. PT67, a NIH 3T3-derived packaging cell line (Clontech), expressing the viral envelope, was cultured in DMEM supplemented with 10% FBS. For vector production, PT67 packaging cells, at 70% confluence, were incubated with a precipitated mixture of LipofectAMINE reagent (Life Technologies) and saturating amounts of pLNCX2-DsRed2 plasmid for 18 h. Fresh medium was replenished at this time. The cells were examined by fluorescence microscopy 48 h post-transduction. For selection of a clone producing high amounts of RFP retroviral vector (PT67-DsRed2), the cells were cultured in the presence of 200 to 1,000 μg/mL G418 (Life Technologies) for 7 d. The isolated packaging cell clone was termed PT67-DsRed2 (12–15).

***RFP* Gene Transduction of Cancer Cells.** For *RFP* gene transduction, cancer cells were incubated with a 1:1 precipitated mixture of retroviral supernatants of PT67-DsRed2 cells and RPMI 1640 containing 10% FBS for 72 h. Fresh medium was replenished at this time. Tumor cells were harvested with trypsin/EDTA 72 h post-transduction and subcultured at a ratio of 1:15 into selective medium, which contained 200 μg/mL G418. To select brightly fluorescent cells, the level of G418 was increased up to 800 μg/mL in a stepwise manner. RFP-expressing cancer cells were isolated with cloning cylinders (Bel-Art Products) using trypsin/EDTA. Cells were amplified by conventional culture methods in the absence of selective agent (12–15).

Animal Experiments. Athymic nude mice were kept in a barrier facility under HEPA filtration. Mice were fed with autoclaved laboratory rodent diet (Tecklad LM-485, Western Research Products). All animal studies were conducted in accordance with the principals and procedures outlined in the National Institutes of Health Guide for the Care and Use of Laboratory Animals under assurance A3873–01.

Subcutaneous Tumor Model. Subcutaneous tumors were produced by injection of 3×10^6 noncolored PC-3 or PC-3-RFP human prostate cancer cells in 5-week old nude mice. When tumors reached approximately 6 mm in diameter, the tumors were intratumorally injected with PBS for control or OBP-401 at a dose of 1×10^8 PFU in 100 μL PBS. Mice were examined for fluorescence expression with a long-pass filter (a filter for simultaneous observation of both GFP and RFP) or with specific filters for GFP or RFP.

Peritoneal Carcinomatosis Model of HCT-116 Human Colon Cancer Cells. Five-week-old nude mice were i.p. injected with noncolored HCT-116 or HCT-116-RFP human colon cancer cells (3×10^6 in 200 μL HBSS) using a 27-gauge needle. Twelve days after cancer cell inoculation, mice were injected i.p. with OBP-401 at a dose of 1×10^8 PFU in 200 μL PBS. Five days after virus injection, the abdominal cavity was directly examined by fluorescence imaging under anesthesia.

Pleural Carcinomatosis Model of A549 Human Lung Cancer Cells. Five-week-old nude mice were inoculated with noncolored A549 cells (2×10^6 cells in 200 μL HBSS) into the thoracic space using a 27-gauge needle. Ten days after cancer cell inoculation, OBP-401 at a dose of 1×10^8 PFU in 200 μL PBS was intrapleurally injected. Five days after virus injection, the pleural cavity was directly imaged for GFP expression. GFP-expressing tissues were removed and examined microscopically.

Fluorescence Optical Imaging and Processing. An Olympus OV100 Small Animal Imaging System containing an MT-20 light source was used. High-resolution images were captured directly on a PC (Fujitsu Siemens). Images were analyzed with the use of Cell^R software (Olympus Biosystems) (16).

Histological Examination. For histological studies, GFP-expressing tissues were removed at the time of sacrifice and put into buffered formalin for 24 h at room temperature. All of the tissues were subsequently processed through alcohol dehydration and paraffinization. Tissues were embedded in paraffin and sectioned at 5 μm. All slides were stained by H&E, and examined microscopically.

ACKNOWLEDGMENTS. This project was supported in part by National Cancer Institute Grant CA132242.

1. Sugarbaker PH (2004) Managing the peritoneal surface component of gastrointestinal cancer. Part 1. Patterns of dissemination and treatment options. *Oncology* 18:51–59.
2. Sugarbaker PH (2004) Managing the peritoneal surface component of gastrointestinal cancer. Part 2. Perioperative intraperitoneal chemotherapy. *Oncology* 18:207–219.
3. Glehen O, et al. (2004) Cytoreductive surgery combined with perioperative intraperitoneal chemotherapy for the management of peritoneal carcinomatosis from colorectal cancer: A multi-institutional study. *J Clin Oncol* 22:3284–3292.
4. Kawashima T, et al. (2004) Telomerase-specific replication-selective virotherapy for human cancer. *Clin Cancer Res* 10:285–292.
5. Taki M, et al. (2005) Enhanced oncolysis by a tropism-modified telomerase-specific replication-selective adenoviral agent OBP-405 ('Telomelysin-RGD'). *Oncogene* 24:3130–3140.
6. Umeoka T, et al. (2004) Visualization of intrathoracically disseminated solid tumors in mice with optical imaging by telomerase-specific amplification of a transferred green fluorescent protein gene. *Cancer Res* 64:6259–6265.
7. Kishimoto H, et al. (2006) In vivo imaging of lymph node metastasis with telomerase-specific replication-selective adenovirus. *Nat Med* 12:1213–1219.
8. Fujiwara T, et al. (2006) Enhanced antitumor efficacy of telomerase-selective oncolytic adenoviral agent OBP-401 with docetaxel: Preclinical evaluation of chemovirotherapy. *Int J Cancer* 119:432–440.
9. Sadeghi B, et al. (2000) Peritoneal carcinomatosis from non-gynecologic malignancies: Results of the EVOCAPE 1 multicentric prospective study. *Cancer* 88:358–363.
10. Stepp H, et al. (2007) ALA and malignant glioma: Fluorescence-guided resection and photodynamic treatment. *J Environ Pathol Toxicol Oncol* 26:157–164.
11. Yang M, Luiken G, Baranov E, Hoffman RM (2005) Facile whole-body imaging of internal fluorescent tumors in mice with an LED flashlight. *Biotechniques* 39:170–172.
12. Hoffman RM (2005) The multiple uses of fluorescent proteins to visualize cancer in vivo. *Nat Rev Cancer* 5:796–806.
13. Hoffman RM, Yang M (2006) Subcellular imaging in the live mouse. *Nature Protoc* 1:775–782.
14. Hoffman RM, Yang M (2006) Color-coded fluorescence imaging of tumor-host interactions. *Nature Protoc* 1:928–935.
15. Hoffman RM, Yang M (2006) Whole-body imaging with fluorescent proteins. *Nature Protoc* 1:1429–1438.
16. Yamauchi K, et al. (2006) Development of real-time subcellular dynamic multicolor imaging of cancer-cell trafficking in live mice with a variable-magnification whole-mouse imaging system. *Cancer Res* 66:4208–4214.

A simple biological imaging system for detecting viable human circulating tumor cells

Toru Kojima,[1,2] Yuuri Hashimoto,[1,3] Yuichi Watanabe,[1,3] Shunsuke Kagawa,[1,2] Futoshi Uno,[1,2] Shinji Kuroda,[1,2] Hiroshi Tazawa,[2] Satoru Kyo,[4] Hiroyuki Mizuguchi,[5] Yasuo Urata,[3] Noriaki Tanaka,[1] and Toshiyoshi Fujiwara[1,2]

[1]Division of Surgical Oncology, Department of Surgery, Okayama University Graduate School of Medicine, Dentistry and Pharmaceutical Sciences, Okayama, Japan. [2]Center for Gene and Cell Therapy, Okayama University Hospital, Okayama, Japan. [3]Oncolys BioPharma Inc., Tokyo, Japan. [4]Department of Obstetrics and Gynecology, Kanazawa University School of Medicine, Kanazawa, Japan. [5]Department of Biochemistry and Molecular Biology, Graduate School of Pharmaceutical Sciences, Osaka University, Osaka, Japan.

The presence of circulating tumor cells (CTCs) in the peripheral blood is associated with short survival, making the detection of CTCs clinically useful as a prognostic factor of disease outcome and/or a surrogate marker of treatment response. Recent technical advances in immunocytometric analysis and quantitative real-time PCR have made it possible to detect a few CTCs in the blood; however, there is no sensitive assay to specifically detect viable CTCs. Here, we report what we believe to be a new approach to visually detect live human CTCs among millions of peripheral blood leukocytes, using a telomerase-specific replication-selective adenovirus expressing GFP. First, we constructed a GFP-expressing attenuated adenovirus, in which the telomerase promoter regulates viral replication (OBP-401; TelomeScan). We then used OBP-401 to establish a simple ex vivo method that was able to detect viable human CTCs in the peripheral blood. The detection method involved a 3-step procedure, including the lysis of rbc, the subsequent addition of OBP-401 to the cell pellets, and an automated scan using fluorescence microscopy. OBP-401 infection increased the signal-to-background ratio as a tumor-specific probe, because the fluorescent signal was amplified only in viable, infected human tumor cells, by viral replication. This GFP-expressing virus-based method is remarkably simple and allows precise enumeration of CTCs.

Introduction

Determination of the extent of the disease is the most important factor in predicting the clinical outcome in cancer patients. Primary cancers have been known to shed tumor cells into the blood circulation, which represents the route for systemic tumor cell dissemination (1, 2). Indeed, the presence of circulating tumor cells (CTCs) in the peripheral blood is associated with short survival, and therefore the detection of CTCs is clinically useful as a prognostic factor of disease outcome and/or as a surrogate marker of treatment response (3, 4). Technical advances in immunocytometric analysis and quantitative real-time PCR have made it possible to detect a few CTCs in the blood; however, background expression of cancer-associated antigens, such as cytokeratin 8 (CK-8), CK-18, and CK-19, in normal epithelial cells results in the false-positive detection, and PCR-based methods can not permit analysis of cell morphology. Moreover, there is no sensitive assay for detecting viable CTCs.

The GFP, which was originally identified from the jellyfish *Aequorea victoria*, is an attractive molecular marker for imaging in live tissues because of the relatively noninvasive nature of fluorescent (5–8). It has been reported that hormone-refractory human prostate carcinoma, growing orthotopically in nude mice, efficiently deliver viable tumor cells in the host circulation, which could be detectable using the fluorescence microscopy, when marked by GFP expression (9). In addition, isolated rare CTCs showed an increased metastatic propensity. We reported previously that intratumoral injection of telomerase-specific replication-selective adenovirus expressing the *gfp* gene (OBP-401; TelomeScan) causes viral spread into the regional lymphatics, with subsequent selective replication in neoplastic lesions, resulting in GFP expression in metastatic lymph nodes in *nu/nu* mice (10). The present study extended our previous work, by developing what we believe to be a novel and simple strategy to selectively label human CTCs with fluorescence among millions of peripheral blood leukocytes. The detection method involves 3-steps: the lysis of rbc, the subsequent addition of OBP-401 to the cell pellets, and the automated scan under the fluorescence microscope. This method allows precise enumeration of human CTCs, because OBP-401 can replicate and express GFP fluorescence only in viable tumor cells.

Results

Selective GFP expression in human cancer cells in vitro by OBP-401. OBP-401 (TelomeScan) was constructed by inserting the *gfp* gene under the control of the CMV promoter at the deleted E3 region of the telomerase-specific replication-selective type 5 adenovirus OBP-301 (Telomelysin) (11, 12) (Figure 1). To determine whether telomerase activity is associated with selective GFP expression in different cancer cell lines, we measured human telomerase reverse transcriptase (*hTERT*) mRNA and GFP expression using quantitative real-time RT-PCR analysis and fluorescence microplate reader, respectively. The *hTERT* expression was directly proportional to the fluorescence intensity, and regression analysis confirmed a strong correlation between these numbers ($r^2 > 0.94$) (Figure 1B). H1299 human non–small cell lung cancer cells expressed bright GFP fluorescence as early as 12 hours after OBP-401 infection, and a positive signal for GFP was detected in all cells at 48 hours after infec-

Conflict of interest: Yasuo Urata is an employee of Oncolys BioPharma Inc., the manufacturer of OBP-401 (TelomeScan).

Citation for this article: *J. Clin. Invest.* doi:10.1172/JCI38609.

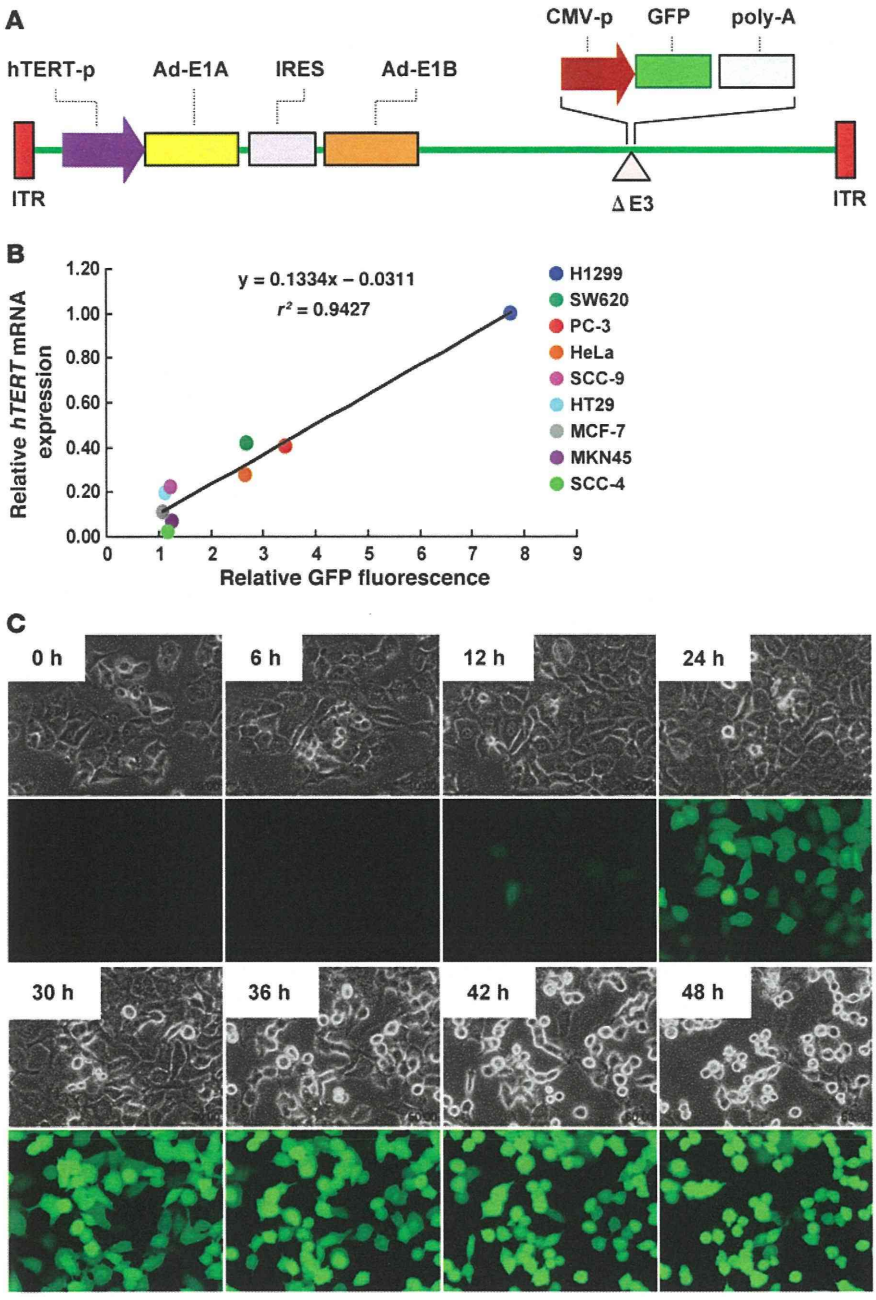

Figure 1
Schematic DNA structure of OBP-401 and selective replication of OBP-401 in human cancer cells. (**A**) OBP-401 is a telomerase-specific replication-competent adenovirus variant, in which the hTERT promoter element drives expression of the *E1A* and *E1B* genes linked with an IRES, and the *gfp* gene is inserted under the CMV promoter into the E3 region for monitoring viral replication. hTERT-p, hTERT promoter; Ad-E1A, adenoviral E1A; Ad-E1B, adenoviral E1B; CMV-p, CMV promoter; poly-A, polyadenylation signal; ITR, inverted terminal repeat. (**B**) Relationship between *hTERT* expression and GFP fluorescence. Relative *hTERT* mRNA expression and GFP fluorescence in human tumor cell lines were determined by real-time RT-PCR analysis and fluorescence microplate reader, respectively. The relative *hTERT* mRNA expression ratios normalized by dividing the value of H1299 cells are presented for each sample. Relative GFP fluorescence was measured 48 hours after OBP-401 infection at an MOI of 10. (**C**) Time-lapse images of H1299 human lung cancer cells were recorded for 48 hours after OBP-401 infection at an MOI of 10. Selected images taken at the indicated time points show cell morphology by phase-contrast microscopy (top panels) and GFP expression under fluorescence microscopy (bottom panels). Original magnification, ×200.

tion (Figure 1C and Supplemental Video 1; supplemental material available online with this article; doi:10.1172/JCI38609DS1). OBP-401 infection also induced GFP expression in other neoplastic cells such as human sarcoma cell lines within 24 hours after infection (Supplemental Figure 1 and Supplemental Video 2). In parallel experiments, OBP-401 infection induced dose-dependent GFP expression in a variety of human cancer cell lines that originated from different organs (Supplemental Figure 2).

Measurement of viable CTCs with OBP-401 in the blood. We used OBP-401 to establish a simple ex vivo method for detecting viable human CTCs in the peripheral blood. As illustrated in Figure 2A, the method involves a 3-step procedure, including the lysis of rbc in 5-ml aliquots of whole blood samples, subsequent addition of 10^4 PFUs of OBP-401 to the cell pellets, and the deposition of cells on polylysine-coated slides, followed by automated scanning under a fluorescence microscope. OBP-401 infection increases the signal-to-background ratio as a tumor-specific probe, because the fluorescent signal can be amplified only in tumor cells by telomerase-specific viral replication. The automated optical scan system provides high speed and accuracy of slide movement in all x, y, and z directions for the acquisition of a large number of high-resolution segmented tile images, at a magnification of ×100 for each tile (Figure 2B). Each optical field is focused automatically before image acquisition. The captured segmented tile images are automatically combined to construct a large image, with a total area of 20 × 20 mm. Since each tile segment can be magnified without the loss of high resolution, OBP-401–infected human tumor cells could be easily visualized with GFP signals in blood smears (Figure

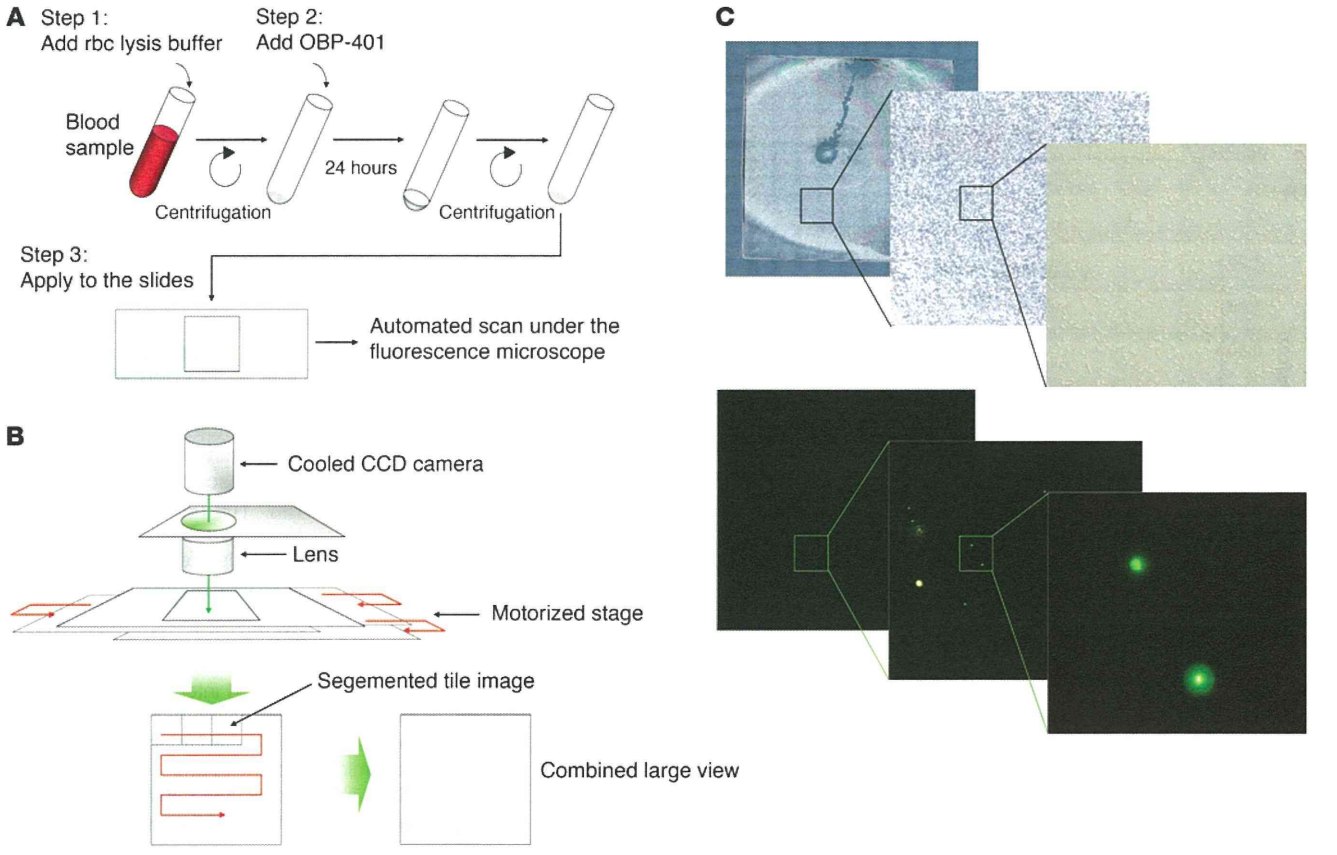

Figure 2

A simple method to detect telomerase-positive cells in the blood. (**A**) Steps in the sample preparation for GFP fluorescence detection. Blood samples (5-ml samples) are collected in heparinized tubes and incubated with rbc lysis buffer containing ammonium chloride (NH_4Cl) for 15 minutes. After centrifugation, cell pellets are mixed with 10^4 PFUs of OBP-401 and incubated at room temperature for another 24 hours. Cells are resuspended in 15 μl of PBS following centrifugation and then placed onto the slide under a coverslip. (**B**) System for automated fluorescence molecular imaging. The automated optical scan system serially captures segmented tile images in the area of the coverslip under fluorescence microscopy. (**C**) A high-resolution large view of the reconstructed tile images. The zoomed image allows easy visualization of GFP-expressing cells among millions of blood leukocytes. Original magnification, ×40 (left panels); ×100 (middle panels); ×400 (right panels).

2C). This automated microscopic scan system allows us to obtain high-magnification images with a large field of view.

Accuracy of CTC detection by ex vivo OBP-401 infection. To test the efficacy and accuracy of the system, whole blood samples from healthy donors were spiked with variable numbers of H1299 human lung cancer cells and then analyzed. Representative images of each sample are shown in Figure 3A. H1299 cells could be distinguished from the other blood cells even at lower magnification. The recovery of tumor cells was consistent over a target frequency range, between 10 and 1,000 cells spiked into 5 ml of blood from normal donors. Regression analysis of the number of GFP-positive cells versus the number of expected tumor cells yielded a correlation coefficient of $r^2 = 0.9996$ (Figure 3B). Thus, the number of GFP-positive cells reflects the actual peripheral blood tumor cell load. We also performed immunohistochemical analysis with anti-human CK-7/8 antibody to ensure that the cells labeled with GFP signals were indeed tumor cells. We used CK-7/8 as a marker for tumor cell detection, as H1299 cells were completely negative for CK-19 (Supplemental Figure 3). The automated microscopic scan system permits repeated scanning of the same fields repeatedly by a 2-dimensional line scanning technology. Merged images of fluorescent detection and CK-7/8 immunostaining confirmed that H1299 human lung cancer cells stably transfected with the *gfp* gene were CK-7/8 positive in the blood smear (Supplemental Figure 3). By using this dual imaging method, we confirmed that the GFP-positive cells were CK-7/8 positive following 24-hour exposure to OBP-401 and were distinguishable from other blood cells (Figure 3C). GFP-expressing cells were also morphologically classified as tumor cells (data not shown).

Comparative analysis of CTC detection by OBP-401, real-time RT-PCR, and flow cytometry. To compare the GFP-based CTC detection and other existing methods, blood samples spiked with variable numbers of H1299 cells were also analyzed. We performed real-time RT-PCR analysis with primers targeting the *hTERT* gene, as OBP-401–mediated GFP expression reflects the telomerase activity (Figure 1B). The number of GFP-positive cells was proportional to the increasing number of H1299 cells, between 10 and 1,000 cells in 5 ml of blood after ex vivo OBP-401 infection (Figure 3B); a significant increase in amplification, however, could not be observed even with 2,000 tumor cells in 1 ml of blood by real-time RT-PCR (Figure 4A), suggesting that the detected *hTERT* mRNA levels might be the background expression. In addition, a

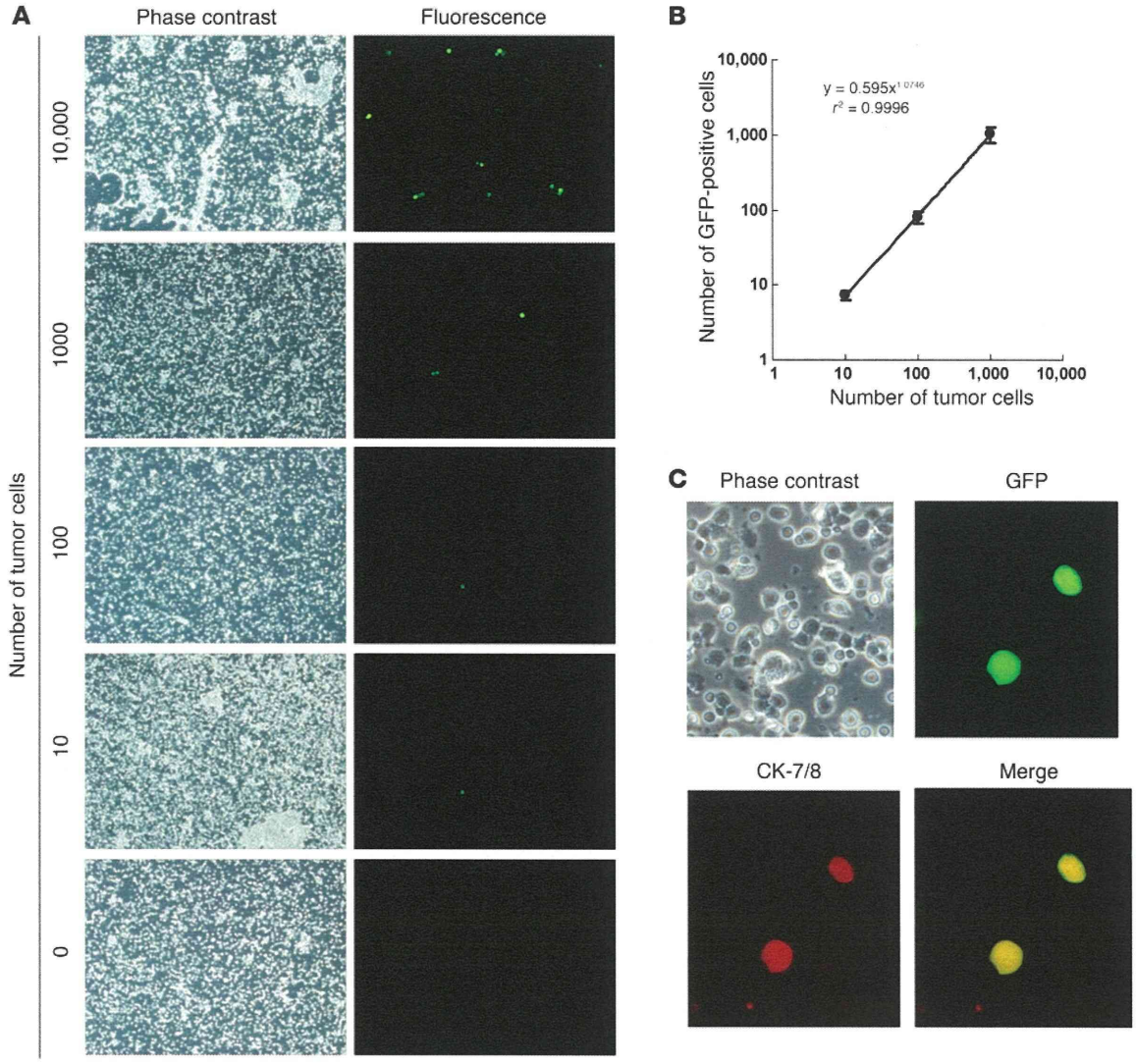

Figure 3
Selective visualization of human cancer cells by OBP-401. (**A**) Phase-contrast and fluorescent images of peripheral blood cells mixed with H1299 human lung cancer cells. Variable numbers of H1299 cells were spiked into 5 ml of whole blood samples from healthy donors and then immediately analyzed for GFP expression. Original magnification, ×100. (**B**) Efficiency of labeling tumor cells added to whole human blood with OBP-401. The number of tumor cells spiked into whole blood versus the number of GFP-expressing cells is plotted. Each value represents the mean ± SD. (**C**) Immunohistochemical staining of GFP-expressing cells for CK-7/8. The blood samples mixed with H1299 cells were analyzed for GFP expression, fixed with 2% glutaraldehyde, and then stained with rhodamine-labeled anti–CK-7/8 antibody. Overlap of green (GFP) and red (CK-7/8) fluorescence was displayed as yellow fluorescence. Original magnification, ×600.

quantitative RT-PCR assay could not detect *CK7* mRNA expression in all samples tested (Figure 4B), although H1299 cells were positive for CK-7/8 (Supplemental Figure 4). We also used flow cytometry to detect H1299 tumor cells in the blood; however, the number of GFP-positive cells following ex vivo OBP-401 infection was much lower than expected (Supplemental Figure 4 and Figure 4C). These results suggest that enrichment of tumor cells or depletion of unwanted cells is necessary for CTC detection by real-time RT-PCR and flow cytometry.

Viable CTCs detected with OBP-401 in patients with various cancers. To examine whether CTCs from cancer patients can be labeled with GFP signals by OBP-401 replication to permit their detection in whole blood, we analyzed fresh blood samples collected from 37 patients with histologically confirmed gastric cancer and 9 patients with other malignancies, including colon cancer, hepatocellular carcinoma (HCC), breast cancer, and non–small cell lung cancer. Although the CTC level varied widely, ranging from 0 to 47 cells in 5-ml samples, 26 gastric cancer patients (70.3%) had more than 1 CTC; there was, however, no apparent relationship between CTC counts and TNM stages (Figure 5A, Table 1, and Supplemental Table 1). CTCs were also identified in samples from 6 of 9 (66.7%) patients with other cancers. The number of CTCs that were isolated ranged from 0 to 56 cells per 5-ml sample (Figure 5B, Table 1, and Supplemental Table 2).

To confirm the infectivity of OBP-401 to tumor cells at the primary sites, we applied this assay to single-cell suspensions isolated

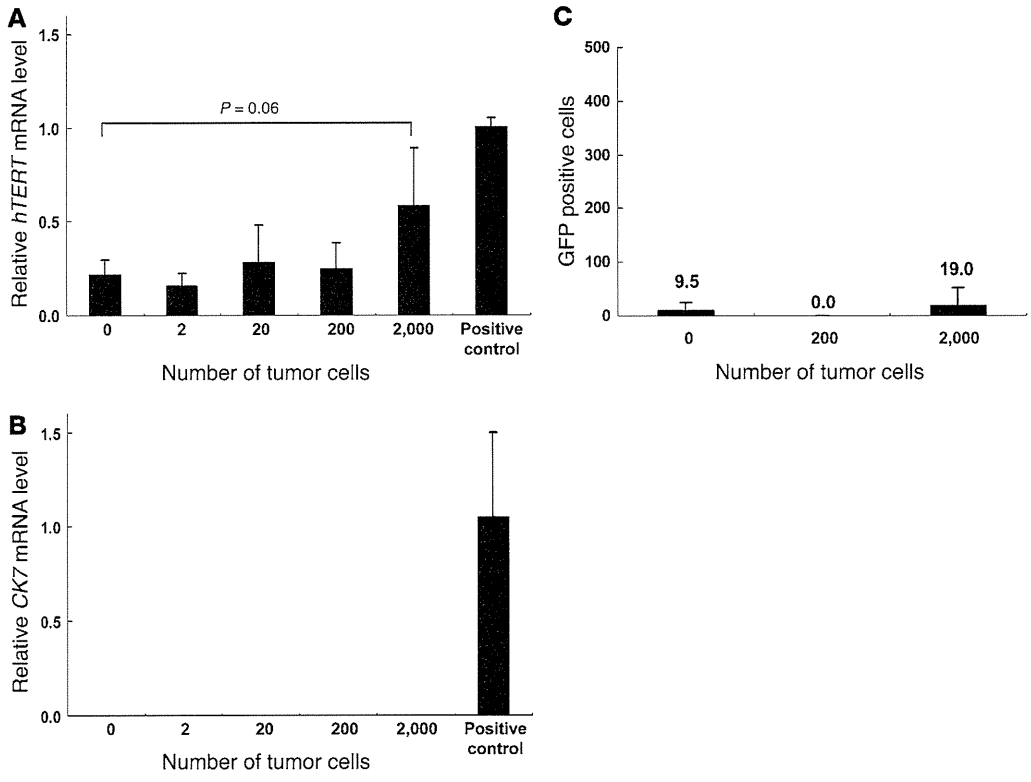

Figure 4

Comparison of the sensitivity of CTC detection by real-time RT-PCR and flow cytometry. (**A** and **B**) Variable numbers of H1299 cells spiked into 1 ml of whole blood samples from healthy donors were prepared. The relative expression of *hTERT* (**A**) and *CK7* (**B**) mRNA was determined by real-time RT-PCR analysis. The amount of *hTERT* and *CK7* mRNA was normalized with data from the real-time amplification of the *GAPDH* housekeeping gene. The blood without H1299 cells was used as a negative control, and H1299 cells without the blood were used as a positive control. (**C**) Flow-cytometric enumeration of variable numbers of H1299 cells mixed in 1 ml of blood samples. After the lysis of rbc, blood samples were infected with 10^4 PFUs of OBP-401 for 24 hours, and then subjected to flow-cytometric analysis. The numbers above the bars indicate the actual numbers of GFP-positive cells. Each value represents the mean ± SD of triplicate experiments.

from surgically removed primary tumors. A gallery of cellular images showed sufficient GFP expression in tumor cells obtained from gastric and colon cancer patients, following OBP-401 infection at a MOI of 100 (Figure 6). The size and morphology of GFP-labeled cells isolated from primary tumors were consistent with those of CTCs detected in the peripheral blood of the same patients.

We further assessed the CTC dynamics in patients who were undergoing chemotherapy or surgery, to demonstrate the clinical potential of our approach for monitoring treatment responses. The results from a representative patient with advanced stage IV gastric cancer (case 1) are shown in Figure 7A. A 5-ml blood sample contained 6 CTCs before treatment. Fourteen days after the initiation of systemic chemotherapy, 7 CTCs were detected in the peripheral blood; the patient, however, had no CTCs after 2 cycles of chemotherapy. A patient who had a recurrence of gastric cancer in the regional lymph nodes (case 10) had decreased CTC counts after a cycle of chemotherapy (Figure 7B). Elimination or reduction of CTCs correlated well with a decrease in the levels of tumor markers such as CEA, CA19-9, and CA125. In contrast, the number of CTCs gradually increased in an advanced gastric cancer patient (case 25) who developed retroperitoneal tumor invasion despite chemotherapy (data not shown). As this patient showed no elevated levels of tumor markers, the kinetic of CTC numbers would enable a faster prediction of the treatment response than that of other radiographic imaging methods. In the 4 patients who underwent surgery (gastric cancer, cases 5 and 9; colon cancer, cases 3 and 4), the CTC level dropped 4 weeks after complete resection (Figure 7, C and D). These results suggest that enumeration of CTCs might be useful for monitoring the efficacy of local and systemic treatments.

Discussion

Early and accurate evaluation of therapeutic efficacy is the hallmark of successful cancer treatment. We have described a simple method, without any complicated processing steps, for detecting viable human CTCs in the peripheral blood, by using telomerase-specific GFP-expressing adenovirus. Viable CTCs may be a less-invasive, repeatable biomarker for monitoring tumor responses against various types of therapies, although its clinical significance is still debatable. In our pilot study, reported herein, serial blood sampling demonstrated that surgical removal of primary tumors was associated with decreased CTC counts. Thus, quantitative detection of CTCs can be also a substantial surrogate marker for treatment efficacy in candidates for chemotherapy.

The technical platform of CTC enumeration has improved rapidly (13). PCR-based techniques, which are commonly used to detect CTCs (14, 15), can detect dead tumor cells and cell-free circulating DNA or RNA, which may result in overestimation of the neoplastic

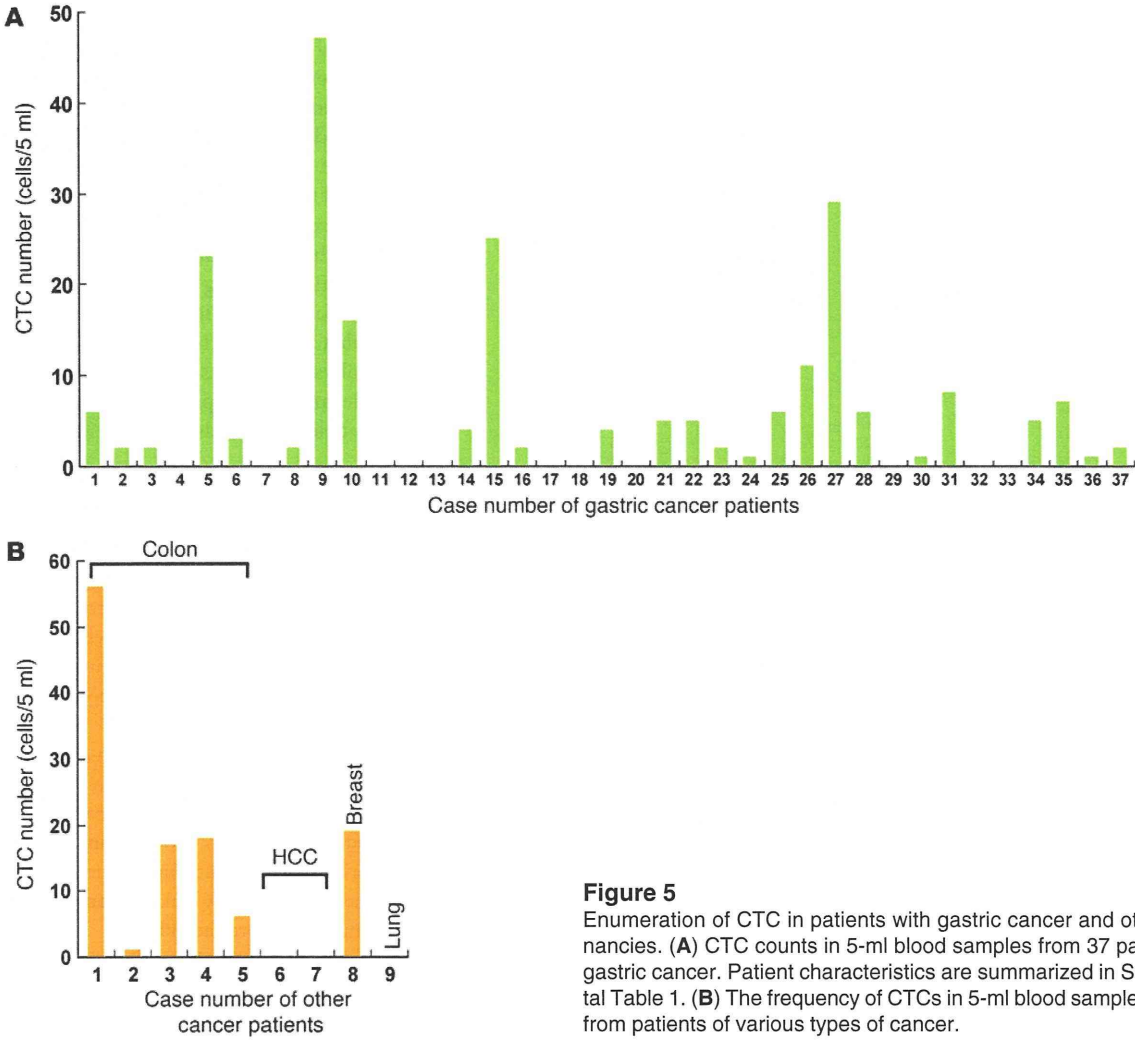

Figure 5
Enumeration of CTC in patients with gastric cancer and other malignancies. (**A**) CTC counts in 5-ml blood samples from 37 patients with gastric cancer. Patient characteristics are summarized in Supplemental Table 1. (**B**) The frequency of CTCs in 5-ml blood samples obtained from patients of various types of cancer.

state. In addition, our data demonstrated that neither quantitative RT-PCR for *hTERT* mRNA nor that for *CK7* mRNA could identify as many as 2,000 human tumor cells per 1 ml of blood without enrichment. Recently, Diehl et al. have reported that circulating tumor DNA is useful as a measure of tumor dynamics and that it can be beneficial for monitoring many types of human cancer (16). Although the system has the ability to quantify the level of circulating DNA and the sufficient sensitivity to detect very small amount of nucleic acids, it requires the identification of a somatic mutation in the individual tumor by sequencing of DNA. Our GFP-based fluorescence imaging can allow simple detection of target cancer cells, without any time-consuming steps, and it seems to be much more reliable and sensitive.

To date, various approaches have been also used to visually identify CTCs; however, the techniques employed to perform cell enrichment, immunohistochemical detection, and image analysis are complicated (17–19). Moreover, epithelial markers are currently used to detect CTCs; tumor cells, however, may lose their epithelial features during metastasis/dissemination or may not express these markers because of their heterogeneity (20). Indeed, the human non–small cell lung cancer cells that we used lack CK-19 expression, which is the marker most extensively studied for the detection of CTCs. The mechanism by which epithelial cells acquire the motile properties is epithelial-to-mesenchymal transition (EMT), a process that is currently popular for investigators of the onset of cancer cell migration, invasion, and metastatic dissemination (21, 22). EMT also promotes cytoskeletal rearrangement in tumor cells, which results in the downregulation of epithelial markers and upregulation of mesenchymal markers (22, 23). Nagrath et al. developed a unique microfluidic platform (CTC-chip) for CTC separation by using anti-epithelial cell adhesion molecule (EpCAM) antibody, and they demonstrated sensitive real-time monitoring of responses to cancer therapy with this technology (24); the loss of EpCAM expression, however, has been reported in metastatic and drug-resistant cancer cells (25). The multimarker assay may show slightly increased sensitivity for CTC detection over the single-marker method (26, 27); the procedures, however, are complicated. In contrast, telomerase is activated in most human cancers and is known to be associated with their malignant properties (28). Recent studies have reported that EMT can produce the cancer stem cell phenotype (29, 30). Since telomerase activity is one of the stem-cell properties (31), our system may be capable of detecting circulating cancer stem cells, even with EMT features, such as the loss and/or redistribution of the epithelial markers, that are

Table 1
CTC numbers classified by disease stage (as defined by the TNM classification system) and type

Cancer	Stage	GFP-positive cells (per 5 ml)					
		0	1–5	6–10	11–20	21–30	≥31
Gastric	I	5	5	2			1
Gastric	II		4			2	
Gastric	III	3	2	1			
Gastric	IV	3	4	1	2	1	
Colon	I				1		
Colon	II						
Colon	III			1	1		1
Colon	IV		1				
HCC	II	1					
HCC	III	1					
Breast	IV				1		
Lung	I	1					

responsible for metastasis. Moreover, as GFP-positive cells could be collected by flow-cytometric sorting (32), this technology might be applicable for molecular analysis of CTCs.

One of the crucial features that we believe to be unique of our approach is to use the virus with the self-proliferation potency. Although adenovirus-mediated transduction of the reporter genes into target cells is a common strategy in basic research, to the best of our knowledge, this is the first demonstration of ex vivo visualization of live CTCs, with a genetically engineered adenoviral agent, combined with an automated optical scan system for clinical studies. Infection efficiency of the adenoviral agent, which is derived from human adenovirus serotype 5, varies widely depending on the expression of Coxsackie-adenovirus receptor (CAR) (33). This might be one of the potential advantages of our system, because most of human hematopoietic cells are almost refractory to transduction by adenovirus vectors, due to the lack of CAR for virus binding (34). Therefore, when OBP-401 is used to detect CTCs in the peripheral blood, OBP-401 infection is limited in hematopoietic cells, including leukocytes. Moreover, OBP-401 replication is unlikely in normal hematopoietic cells, because of their low telomerase activity.

Our patient data demonstrate that enumeration of CTCs reflects the tumor burden, as the CTC counts decreased upon complete surgical removal of primary tumors. In addition, although the sample size is too small to perform a statistical analysis, 2 gastric cancer patients, who favorably responded to systemic chemotherapy, exhibited a gradual lowering of CTC counts in parallel with a decrease in the level of tumor markers, whereas a radiographically nonresponding patient had an increased CTC count. In contrast, the absolute number of CTCs did not correspond with tumor sizes or TNM stages in patients, and a small number of CTCs (0–4 cells in 5-ml samples) were detected in healthy normal volunteers (data not shown). These results suggest that it is more important to measure the change in CTC quantity, than to simply determine whether the value is below or above a disease-specific cutoff point; the CTC count was, however, mostly analyzed with this endpoint in clinical trials that used immunomagnetic-bead purification (3, 4, 17). Recently, Scher et al. have demonstrated that the use of CTC count as a continuous variable enables the prediction of survival in patients with castration-resistant prostate cancer (35). Although we cannot comment on the prognostic utility of CTC values in the absence of outcome data, our OBP-401–based method is at least useful as a measure of tumor dynamics. A larger series of clinical trials and longer follow-up studies are necessary to confirm the feasibility of this technology.

In conclusion, we developed an ex vivo GFP-based fluorescence imaging system that is very simple and suitable for accurate identification and enumeration of viable CTCs. This technology has the potential to allow physicians to assess the response to treatment as a relevant clinical parameter, especially in patients without elevated levels of tumor markers.

Methods

Cell culture. The human non-small cell lung cancer cell line H1299, the human tongue squamous carcinoma cell lines SCC-4 and SCC-9, the human gastric cancer cell line MKN45, the human colorectal cancer cell lines HT-29 and SW620, the human prostate cancer cell line PC-3, the human cervical adenocarcinoma cell line HeLa, and the human mammary gland adenocarcinoma cell line MCF-7 were cultured according to the specifications supplied by the vendor.

Virus. OBP-401 is a telomerase-specific replication-competent adenovirus variant, in which the hTERT promoter element drives the expression of the *E1A* and *E1B* genes linked with an internal ribosome entry site (IRES), and the *gfp* gene is inserted under the CMV promoter into the E3 region (7, 8, 10). The virus was purified by ultracentrifugation in cesium chloride step gradients, the titer was determined by a plaque-forming assay using 293 cells, and the virus sample was stored at –80°C.

Quantitative real-time RT-PCR analysis. Total RNA from cultured cells was obtained by using the RNeasy Mini Kit (Qiagen). The *hTERT* and *CK7* mRNA copy numbers were determined by real-time quantitative RT-PCR with a StepOnePlus system and TaqMan Gene Expression Assays (Applied Biosystems). Specific primers for hTERT (Hs00972650_m1), CK-7 (Hs00559840_m1), and GAPDH (Hs99999905_m1) were used (Applied Biosystems). PCR amplification began with a 20-second denaturation step at 95°C and then 40 cycles of denaturation at 95°C for 1 second and annealing/extension at 60°C for 20 seconds. Data analysis was performed using StepOne Software (Applied Biosystems). The *GAPDH* housekeeping gene was used as the reference gene for PCR normalization. The ratios normalized by dividing the value of H1299 cells were presented for each sample.

Fluorescence microplate reader. Cells were infected with OBP-401 at the indicated MOI values in a 96-well black-bottom culture plate and then further incubated for the indicated time periods. GFP fluorescence was measured by using a fluorescence microplate reader (DS Pharma Biomedical) with excitation/emission at 485 nm/528 nm. The GFP fluorescence was expressed relative to that of MCF-7 cells.

Time-lapse fluorescence microscopy. Cells were infected with OBP-401 at an MOI of 10 for 2 hours in vitro. Phase-contrast and fluorescent time-lapse recordings were obtained to concomitantly analyze cell morphology and GFP expression with an inverted microscope (Olympus) equipped with a heated stage and controlled CO_2 environment (37°C, 8.5% CO_2) (Tokai Hit). Images were taken every 10 minutes.

Sample preparation and automated optical imaging analysis. A simple 3-step method is used to detect viable human CTCs in the peripheral blood. Briefly, 5-ml blood samples were drawn into heparinized tubes and incubated with lysis buffer containing ammonium chloride (NH_4Cl) for 15 minutes to remove

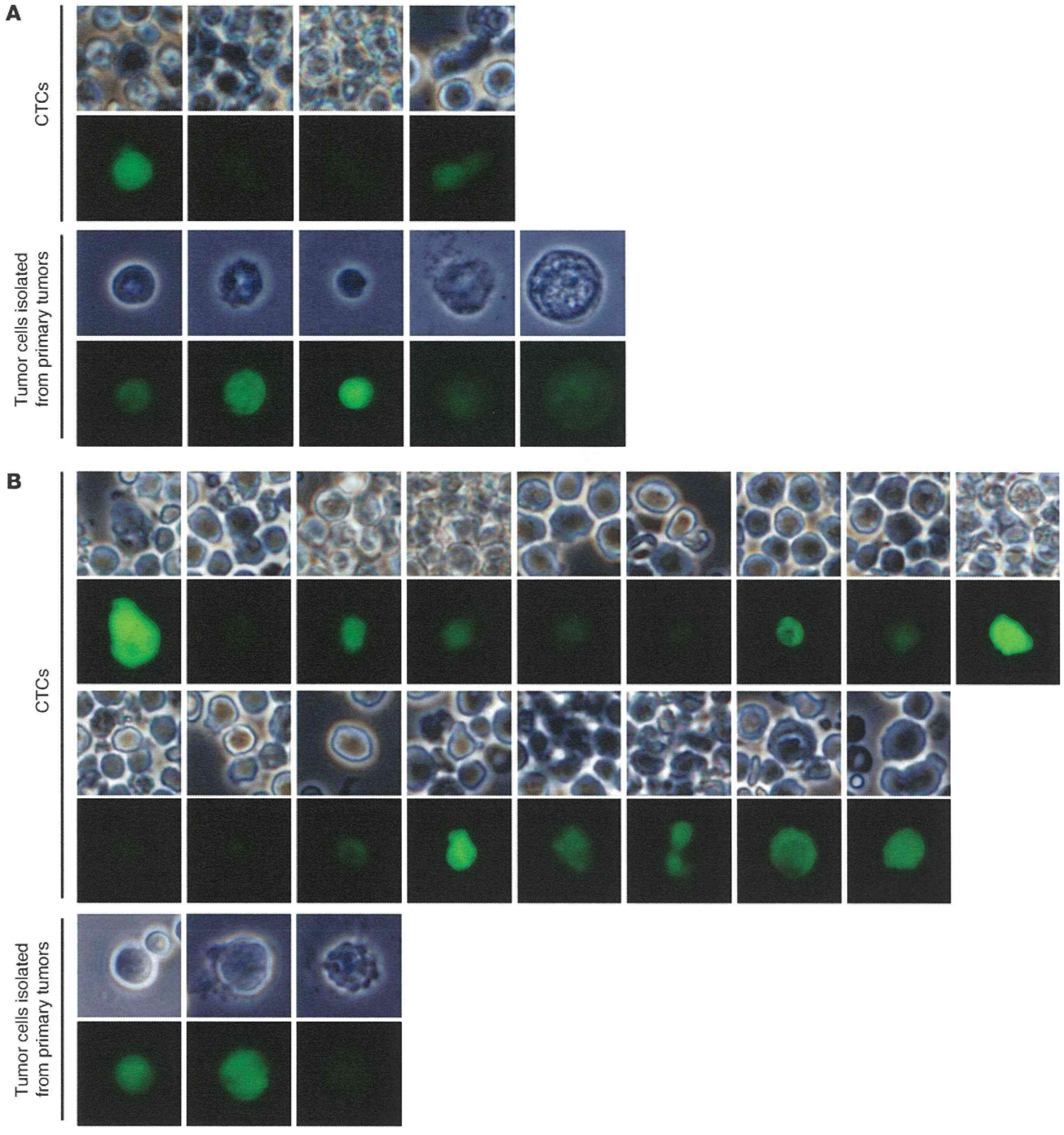

Figure 6
Images of GFP-positive cells obtained from the peripheral blood and the primary tumors. (**A**) CTCs were visualized by GFP expression among peripheral blood leukocytes in the blood sample obtained from a stage Ib gastric cancer patient (case 31). A single-cell suspension was also prepared from surgically removed primary tumor and exposed to OBP-401 at an MOI of 100 for 24 hours. (**B**) Primary tumor cells were also isolated from a patient with stage IIIa colon cancer (case 3) and infected with OBP-401 at an MOI of 100. Cell morphology of CTCs and primary tumor cells is shown by phase-contrast microscopy (first and third rows in **A** and first, third, and fifth rows in **B**), and GFP expression is shown by fluorescence microscopy (second and fourth rows in **A** and second, fourth, and sixth rows in **B**). Original magnification, ×600.

erythrocytes. After centrifugation, the cell pellets were mixed with 10^4 PFUs of OBP-401 and incubated at room temperature for another 24 hours. Following centrifugation, the cells were resuspended in 15 μl of PBS and then placed onto a slide under a coverslip. A motorized stage (Tokai Hit), mounted on a fluorescence microscope, serially captured segmented tile images in the area of the coverslip. The captured segmented tile images were joined together by MetaMorph 7.5, an image acquisition and analysis software (Molecular Devices), to create a large image of a 20-mm × 20-mm area. GFP signals could be

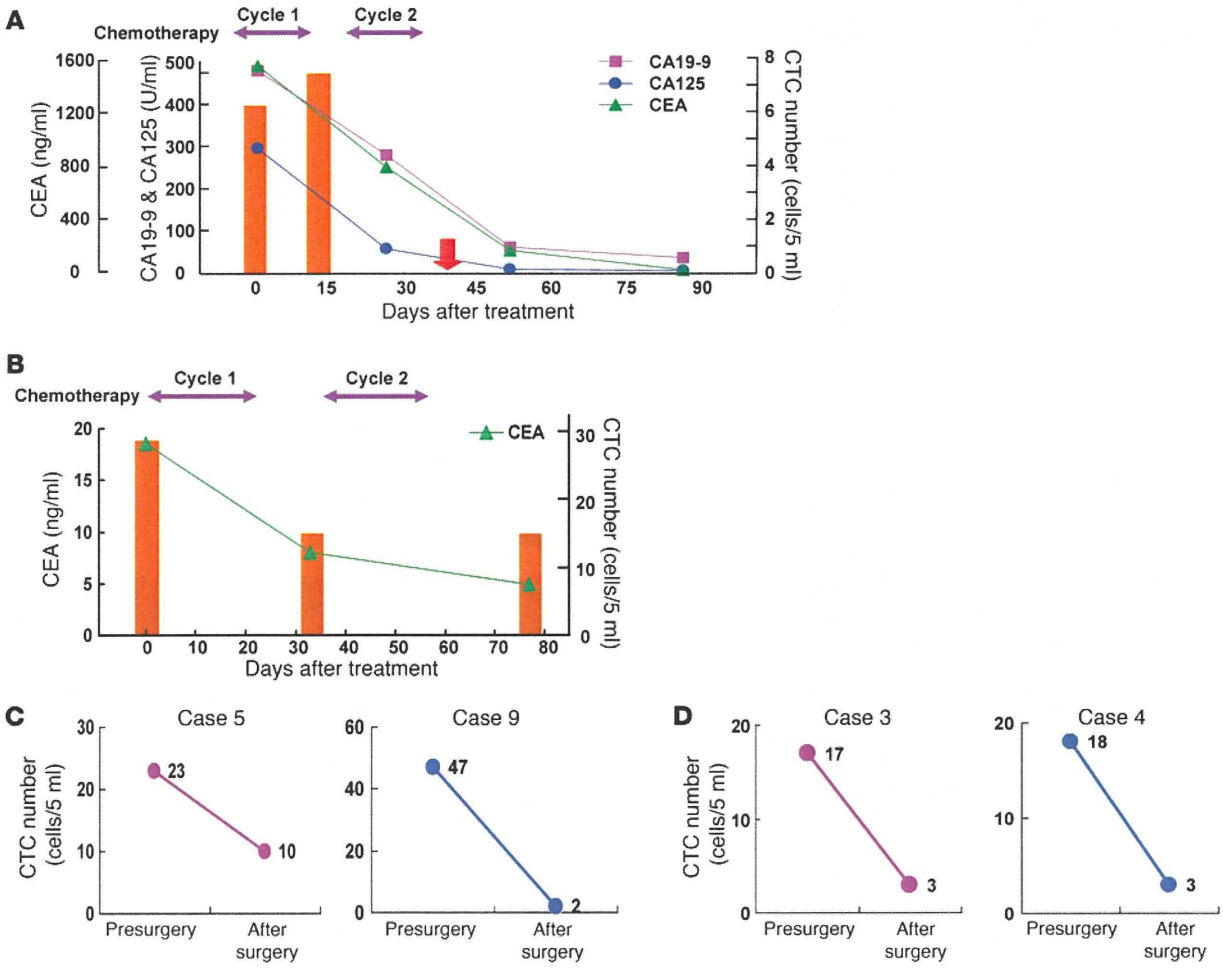

Figure 7

CTC dynamics at baseline and after treatment in patients with gastric or colon cancer. (**A**) Quantitation of CTCs in peripheral blood samples from an advanced gastric cancer patient (case 1) with multiple liver metastases who received 2 cycles of systemic chemotherapy. CTC counts at the indicated time points (orange bars) were plotted along with the levels of tumor markers CEA, CA19-9, and CA125. A decrease in the CTC number from 7 to 0 was observed 38 days after starting chemotherapy (red arrows). (**B**) The patient with recurrent gastric cancer at regional lymph nodes (case 27) was treated with 2 cycles of systemic chemotherapy. The CTC quantity (orange bars) and CEA level were well correlated over the course of treatment. (**C** and **D**) Changes in CTC numbers after surgery. CTC numbers were measured before and 4 weeks after surgical resection of primary tumors and regional lymph node dissection. (**C**) Two gastric cancer patients (cases 5 and 9) underwent a total gastrectomy and distal gastrectomy, respectively. (**D**) Low anterior resection was performed in 2 colorectal cancer patients (cases 3 and 4).

visualized easily in high-magnification images with a large field of view. The institutional review board at Okayama University Graduate School approved the study protocol, and all patients provided written informed consent.

Immunohistochemistry. Cells on the slides were fixed with 2% glutaraldehyde and washed 3 times with PBS. The slides were subsequently incubated with rhodamine-labeled anti-CK-7/8 antibody (CAM5.2; BD Biosciences) for 1 hour at 37°C. After washing 3 times with PBS, the slides were mounted with buffered glycerol for examination by fluorescence microscopy.

Tumor cell preparation. Primary solid tumors were surgically removed from patients with gastric cancer or other types of cancer. The tumor tissue was homogenized by mechanical mincing, and then the cell mixtures were passed through a cell strainer (BD Biosciences — Discovery Labware) and suspended as a single-cell suspension.

Statistics. We used the Student's 2-tailed t test to identify statistically significant differences between groups. Results are reported as mean ± SD. P values of less than 0.05 were considered statistically significant.

Acknowledgments

We thank Daiju Ichimaru and Hitoshi Kawamura for their helpful discussions. We also thank Tomoko Sueishi, Mitsuko Yokota, and Noriko Imagawa for their excellent technical supports. More importantly, we thank all participated patients for their courage and cooperation. This work was supported by Grants-in-Aid from the Ministry of Education, Science, and Culture, Japan and grants from the Ministry of Health and Welfare, Japan.

Received for publication January 16, 2009, and accepted in revised form July 1, 2009.

Address correspondence to: Toshiyoshi Fujiwara, Center for Gene and Cell Therapy, Okayama University Hospital, 2-5-1 Shikata-cho, Okayama 700-8558, Japan. Phone: 81-86-235-7997; Fax: 81-86-235-7884; E-mail: toshi_f@md.okayama-u.ac.jp.

1. Fidler, I.J. 1973. The relationship of embolic homogeneity, number, size and viability to the incidence of experimental metastasis. *Eur. J. Cancer.* **9**:223–227.
2. Liotta, L.A., Kleinerman, J., and Saidel, G.M. 1974. Quantitative relationships of intravascular tumor cells, tumor vessels, and pulmonary metastases following tumor implantation. *Cancer Res.* **34**:997–1004.
3. Cristofanilli, M., et al. 2004. Circulating tumor cells, disease progression, and survival in metastatic breast cancer. *N. Engl. J. Med.* **351**:781–791.
4. Cristofanilli, M., et al. 2005. Circulating tumor cells: a novel prognostic factor for newly diagnosed metastatic breast cancer. *J. Clin. Oncol.* **23**:1420–1430.
5. Hoffman, R.M. 2005. The multiple uses of fluorescent proteins to visualize cancer in vivo. *Nat. Rev. Cancer* **5**:796–806.
6. Umeoka, T., et al. 2004. Visualization of intrathoracically disseminated solid tumors in mice with optical imaging by telomerase-specific amplification of a transferred green fluorescent protein gene. *Cancer Res.* **64**:6259–6265.
7. Watanabe, T., et al. 2006. Histone deacetylase inhibitor FR901228 enhances the antitumor effect of telomerase-specific replication-selective adenoviral agent OBP-301 in human lung cancer cells. *Exp. Cell Res.* **312**:256–265.
8. Fujiwara, T., et al. 2006. Enhanced antitumor efficacy of telomerase-selective oncolytic adenoviral agent OBP-401 with docetaxel: Preclinical evaluation of chemovirotherapy. *Int. J. Cancer.* **119**:432–440.
9. Glinskii, A.B., et al. 2003. Viable circulating metastatic cells produced in orthotopic but not ectopic prostate cancer models. *Cancer Res.* **63**:4239–4243.
10. Kishimoto, H., et al. 2006. In vivo imaging of lymph node metastasis with telomerase-specific replication-selective adenovirus. *Nat. Med.* **12**:1213–1219.
11. Kawashima, T., et al. 2004. Telomerase-specific replication-selective virotherapy for human cancer. *Clin. Cancer Res.* **10**:285–292.
12. Taki, M., et al. 2005. Enhanced oncolysis by a tropism-modified telomerase-specific replication-selective adenoviral agent OBP-405 ('Telomelysin-RGD'). *Oncogene.* **24**:3130–3140.
13. Paterlini-Brechot, P., and Benali, N.L. 2007. Circulating tumor cells (CTC) detection: clinical impact and future directions. *Cancer Lett.* **253**:180–204.
14. Umetani, N., et al. 2006. Prediction of breast tumor progression by integrity of free circulating DNA in serum. *J. Clin. Oncol.* **24**:4270–4276.
15. Li, Y., et al. 2006. Serum circulating human mRNA profiling and its utility for oral cancer detection. *J. Clin. Oncol.* **24**:1754–1760.
16. Diehl, F., et al. 2008. Circulating mutant DNA to assess tumor dynamics. *Nat. Med.* **14**:985–990.
17. Allard, W.J., et al. 2004. Tumor cells circulate in the peripheral blood of all major carcinomas but not in healthy subjects or patients with nonmalignant diseases. *Clin. Cancer Res.* **10**:6897–6904.
18. Half, E., et al. 2004. HER-2 receptor expression, localization, and activation in colorectal cancer cell lines and human tumors. *Int. J. Cancer.* **108**:540–548.
19. Fehm, T., et al. 2002. Cytogenetic evidence that circulating epithelial cells in patients with carcinoma are malignant. *Clin. Cancer Res.* **8**:2073–2084.
20. Willipinski-Stapelfeldt, B., et al. 2005. Changes in cytoskeletal protein composition indicative of an epithelial-mesenchymal transition in human micrometastatic and primary breast carcinoma cells. *Clin. Cancer Res.* **11**:8006–8014.
21. Thiery, J.P. 2002. Epithelial-mesenchymal transitions in tumour progression. *Nat. Rev. Cancer.* **2**:442–454.
22. Yilmaz, M., and Christofori, G. 2009. EMT, the cytoskeleton, and cancer cell invasion. *Cancer Metastasis Rev.* **28**:15–33.
23. Rees, J.R., Onwuegbusi, B.A., Save, V.E., Alderson, D., and Fitzgerald, R.C. 2006. In vivo and in vitro evidence for transforming growth factor-beta1-mediated epithelial to mesenchymal transition in esophageal adenocarcinoma. *Cancer Res.* **66**:9583–9590.
24. Nagrath, S., et al. 2007. Isolation of rare circulating tumour cells in cancer patients by microchip technology. *Nature.* **450**:1235–1239.
25. Frederick, B.A., et al. 2007. Epithelial to mesenchymal transition predicts gefitinib resistance in cell lines of head and neck squamous cell carcinoma and non-small cell lung carcinoma. *Mol. Cancer Ther.* **6**:1683–1691.
26. Xi, L., et al. 2007. Optimal markers for real-time quantitative reverse transcription PCR detection of circulating tumor cells from melanoma, breast, colon, esophageal, head and neck, and lung cancers. *Clin. Chem.* **53**:1206–1215.
27. Ignatiadis, M., et al. 2008. Prognostic value of the molecular detection of circulating tumor cells using a multimarker reverse transcription-PCR assay for cytokeratin 19, mammaglobin A, and HER2 in early breast cancer. *Clin. Cancer Res.* **14**:2593–2600.
28. Blackburn, E.H. 2000. Telomere states and cell fates. *Nature.* **408**:53–56.
29. Santisteban, M., et al. 2009. Immune-induced epithelial to mesenchymal transition in vivo generates breast cancer stem cells. *Cancer Res.* **69**:2887–2895.
30. Dembinski, J.L., and Krauss, S. 2009. Characterization and functional analysis of a slow cycling stem cell-like subpopulation in pancreas adenocarcinoma. *Clin. Exp. Metastasis.* Online publication ahead of print. doi:10.1007/s10585-009-9260-0.
31. Maurelli, R., et al. 2006. Inactivation of p16INK4a (inhibitor of cyclin-dependent kinase 4A) immortalizes primary human keratinocytes by maintaining cells in the stem cell compartment. *FASEB J.* **20**:1516–1518.
32. Maida, Y., et al. 2009. Diagnostic potential and limitation of imaging cancer cells in cytological samples using telomerase-specific replicative adenovirus. *Int. J. Oncol.* **34**:1549–1556.
33. Wickham, T.J., Mathias, P., Cheresh, D.A., and Nemerow, G.R. 1993. Integrins alpha v beta 3 and alpha v beta 5 promote adenovirus internalization but not virus attachment. *Cell.* **73**:309–319.
34. Kawabata, K., Sakurai, F., Koizumi, N., Hayakawa, T., and Mizuguchi, H. 2006. Adenovirus vector-mediated gene transfer into stem cells. *Mol. Pharm.* **3**:95–103.
35. Scher, H.I., et al. 2009. Circulating tumour cells as prognostic markers in progressive, castration-resistant prostate cancer: a reanalysis of IMMC38 trial data. *Lancet Oncol.* **10**:233–239.

Selective metastatic tumor labeling with green fluorescent protein and killing by systemic administration of telomerase-dependent adenoviruses

Hiroyuki Kishimoto,[1,2,3] Yasuo Urata,[5] Noriaki Tanaka,[3] Toshiyoshi Fujiwara,[3,4] and Robert M. Hoffman[1,2]

[1]AntiCancer, Inc.; [2]Department of Surgery, University of California, San Diego, California; [3]Division of Surgical Oncology, Department of Surgery, Okayama University Graduate School of Medicine, Dentistry and Pharmaceutical Sciences; [4]Center for Gene and Cell Therapy, Okayama University Hospital, Okayama, Japan; and [5]Oncolys BioPharma, Inc., Tokyo, Japan

Abstract

We previously constructed telomerase-dependent, replication-selective adenoviruses OBP-301 (Telomelysin) and OBP-401 [Telomelysin-green fluorescent protein (GFP); TelomeScan], the replication of which is regulated by the human telomerase reverse transcriptase promoter. By intratumoral injection, these viruses could replicate within the primary tumor and subsequent lymph node metastasis. The aim of the present study was to evaluate the possibility of systemic administration of these telomerase-dependent adenoviruses. We assessed the antitumor efficacy of OBP-301 and the ability of OBP-401 to deliver GFP in hepatocellular carcinoma (HCC) and metastatic colon cancer nude mouse models. We showed that i.v. administration of OBP-301 significantly inhibited colon cancer liver metastases and orthotopically implanted HCC. Further, we showed that OBP-401 could visualize liver metastases by tumor-specific expression of the *GFP* gene after portal venous or i.v. administration. Thus, systemic administration of these adenoviral vectors should have clinical potential to treat and detect liver metastasis and HCC. [Mol Cancer Ther 2009;8(11):3001–8]

Introduction

Primary and metastatic liver tumors are a common cause of death throughout the world. Hepatocellular carcinoma (HCC), the most common primary liver tumor, is the fifth most common malignancy and the third most frequent cause of cancer death worldwide (1, 2). HCC often metastasizes widely, and distant metastatic sites include lung, bone, adrenals, and brain. The 5-year survival rates of these patients are usually in the range of 16% to 25% (3). Colorectal cancer is also one of the most common tumors worldwide. The liver is the most preferential site for metastasis of colorectal cancer and over half of these patients die from their metastatic liver diseases (4). Therefore, management of the liver metastases is a key factor for colorectal cancer prognosis.

Liver resection is the only potentially curative treatment option available for patients with primary and metastatic liver tumors (5, 6). However, because only a minority of patients with colorectal liver metastases or HCC are candidates for surgery (7–10), new therapeutic agents and innovative approaches for tumor detection are desired.

We previously constructed two conditionally replicating type 5 adenoviruses OBP-301 (Telomelysin) and OBP-401 [Telomelysin-green fluorescent protein (GFP); TelomeScan]. The replication of these viruses is regulated by the human telomerase reverse transcriptase (hTERT) promoter (11–15). hTERT is the catalytic subunit of telomerase, which is highly active in cancer cells but quiescent in most normal somatic cells (16). Therefore, these adenoviruses have tumor-specific replication regulated by the hTERT transcriptional activity. OBP-301 has shown a strong anticancer efficacy in a variety of tumors *in vitro* and *in vivo* (11, 12, 17–19). We also reported that OBP-401 can replicate in and label cancer cells with GFP *in vitro* and *in vivo* and thereby enables imaging of tumor cells by GFP fluorescence *in vivo* (15). Tumor specificity is conferred by selective replication of OBP-401 in the cancer cells. Replication of the virus, and therefore production of GFP, depends on the tumor-specific expression of telomerase. In those studies, however, the virus was administered locally such as by intratumoral injection or administration into a body cavity (thoracic or abdominal cavity). The efficacy of these viruses, when administered systemically, has not been evaluated.

In the present study, we examined the feasibility of systemic administration of OBP-301 and OBP-401 to colorectal liver metastases and to orthotopic HCC tumor in nude mice models, focusing on the antitumor efficacy of OBP-301 and the ability of OBP-401 to selectively induce *GFP* gene expression in cancer cells.

Materials and Methods

Recombinant Adenovirus

We previously constructed OBP-301, in which the hTERT promoter element drives the expression of the *E1A* and *E1B* genes linked with an internal ribosome entry site (11–14).

Received 6/22/09; revised 8/17/09; accepted 9/1/09; published OnlineFirst 11/3/09.

Grant support: National Cancer Institute grant CA132242.

The costs of publication of this article were defrayed in part by the payment of page charges. This article must therefore be hereby marked *advertisement* in accordance with 18 U.S.C. Section 1734 solely to indicate this fact.

Requests for reprints: Robert M. Hoffman, AntiCancer, Inc., San Diego, CA 92111. Phone: 858-654-2555, Fax: 858-268-4175.
E-mail: all@anticancer.com

doi:10.1158/1535-7163.MCT-09-0556

OBP-401, was derived from OBP-301 and also contains the *GFP* gene under the control of the cytomegalovirus promoter, was also constructed previously (15, 20). These viruses were purified by ultracentrifugation in cesium chloride step gradients. Their titers were determined by a plaque-forming assay using 293 cells. The viruses were stored at −80°C.

Cell Culture

The human colorectal cancer cell line HCT-116 and the human HCC cell lines Hep3B and HepG2 were obtained from the American Type Culture Collection. The cells were cultured in RPMI 1640 (Irvine Scientific) supplemented with 10% fetal bovine serum.

GFP Gene Transduction of Cancer Cells

For *GFP* gene transduction of cancer cells, 20% confluent HCT-116 or Hep3B cells were incubated with a 1:1 precipitated mixture of retroviral supernatants of the PT67 GFP-expressing packaging cells and RPMI 1640 containing 10% fetal bovine serum for 72 h. Fresh medium was replenished at this time. Tumor cells were harvested by trypsin/EDTA 72 h post-transduction and subcultured at a ratio of 1:15 into selective medium containing 200 μg/mL G418. The level of G418 was increased up to 800 μg/mL in a stepwise manner. GFP-expressing cancer cells were isolated with cloning cylinders (Bel-Art Products) using trypsin/EDTA and amplified by conventional culture methods in the absence of selective agent.

Animal Experiments

Athymic nude mice were kept in a barrier facility under HEPA filtration and fed with autoclaved laboratory rodent diet (Teklad LM-485; Western Research Products). All animal studies were conducted in accordance with the principles and procedures outlined in the NIH Guide for the Care and Use of Laboratory Animals under assurance no. A3873-1. All animal procedures were done under anesthesia using s.c. administration of a ketamine mixture (10 μL ketamine HCl, 7.6 μL xylazine, 2.4 μL acepromazine maleate, and 10 μL PBS).

Experimental Liver Metastasis Model of Human Colon Cancer

To generate a liver metastasis model, unlabeled HCT-116 or HCT-116-GFP human colon cancer cells were injected

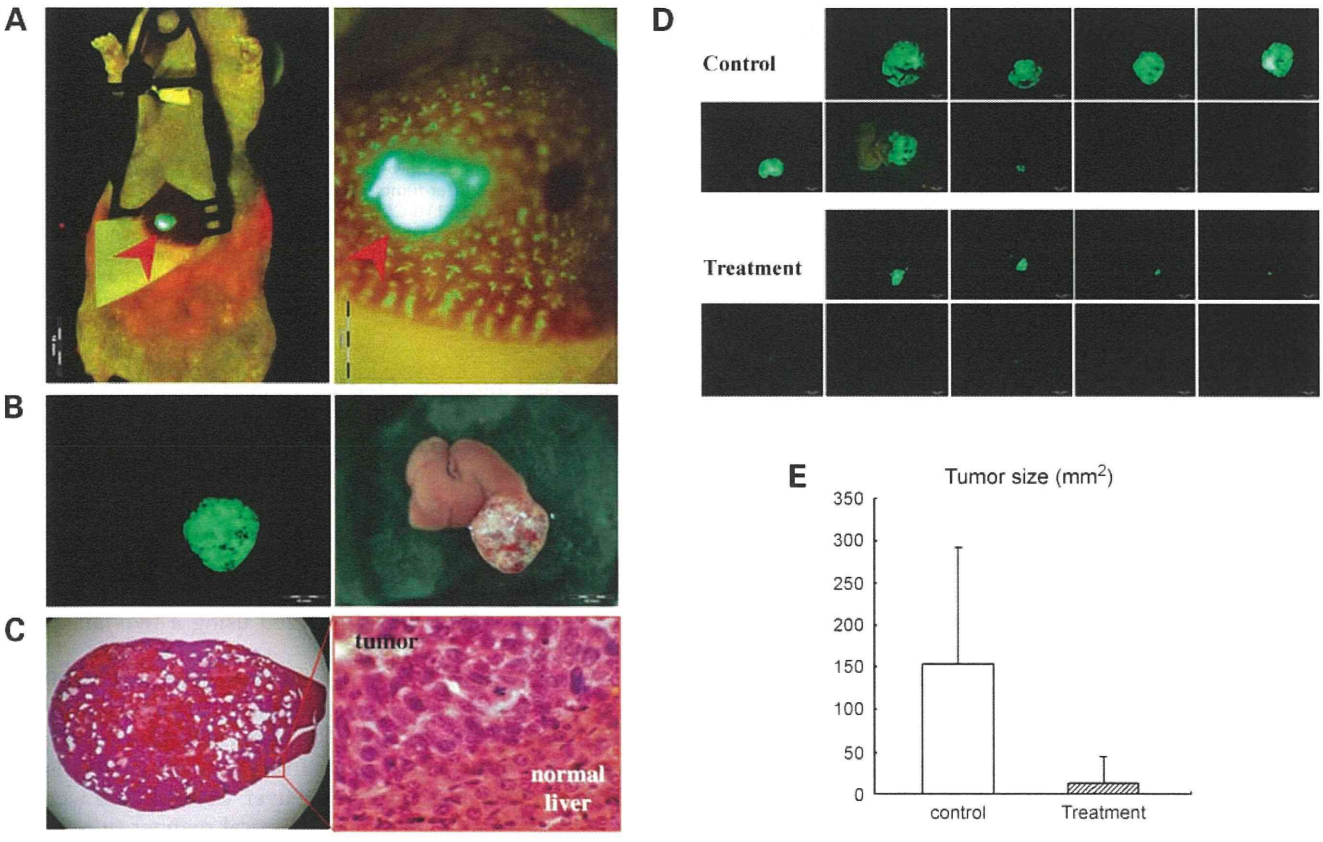

Figure 1. Efficacy of systemic OBP-301 administration on orthotopic HCC. **A,** Hep3B-GFP cells were subserosally injected into the left lobe of the liver (*red arrow*) to generate an orthotopic liver tumor model (*left*). Some cells could be seen accumulating in the terminal portal veins near the bleb of the injected site (*right*). **B,** macroscopic appearance of Hep3B-GFP liver tumor 8 wk after inoculation. *Left,* fluorescence detection; *right,* bright-field observation. **C,** H&E staining of Hep3B-GFP liver tumor section. *Left,* magnification, ×10; *right,* detail of the boxed region. Magnification, ×400. **D,** macroscopic appearance of liver. Livers were excised 8 wk after Hep3B-GFP cells injection. OBP-301 or PBS were i.v. injected biweekly starting from 2 wk after tumor cell inoculation. Excised livers were photographed under fluorescence. **E,** quantitative analysis of the tumor size (fluorescent area) of control and OBP-301–treated mice ($P < 0.01$).

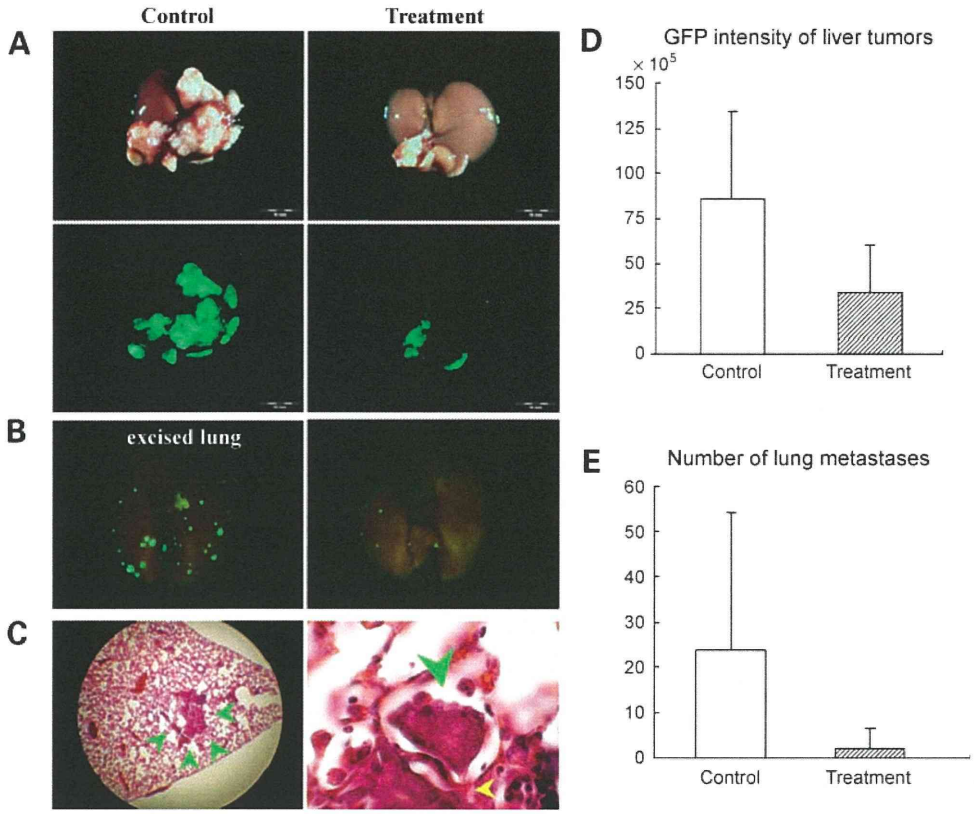

Figure 2. Systemic OBP-301 therapy of colon cancer liver metastases. **A,** macroscopic appearance of livers. HCT-116-GFP cells were injected into the spleen of nude mice, and the liver was excised 6 wk later. OBP-301 or PBS were i.v. injected 5 d after tumor cell inoculation. Excised livers were photographed under bright light (*top*). Fluorescence imaging showed GFP expression signals on the HCT-116-GFP liver metastasis (*bottom*). **B,** macroscopic appearance of lungs. Lung metastatic foci were detected with GFP fluorescence. *Left,* control; *right,* OBP-301 treatment significantly suppressed lung metastasis. **C,** H&E staining of lung metastasis in control mouse (*green arrow*). *Left,* magnification, ×40; *right,* protrusion of tumor (*green arrow*) into the adjacent alveoli through the Kohn's pore (*yellow arrow*). Magnification, ×400. **D,** quantitative analysis of the total GFP intensity in the liver of control and OBP-301–treated mice ($P < 0.05$). **E,** quantitative analysis of the number of lung metastases of control and OBP-301–treated mice ($P < 0.05$).

at a density of 2×10^6 in 50 μL Matrigel (BD Biosciences) into the spleen of nude mice through a 28-gauge needle at laparotomy.

Orthotopic Liver Tumor Model of HCC

An orthotopic liver tumor model with human HCC was made with unlabeled Hep3B or Hep3B-GFP human HCC cells. Unlabeled Hep3B or Hep3B-GFP cells (5.0×10^6 in 10 μL Matrigel) were subserosally injected into the left lobe of the liver through a 28-gauge needle at laparotomy. Unlabeled HepG2 cells, cells (3×10^6 in 50 μL Matrigel) were injected into the spleen of nude mice through a 28-gauge needle at laparotomy.

Antitumor Efficacy Studies

To assess the antitumor efficacy of i.v. administration of OBP-301 against liver metastases of the colorectal cancer, OBP-301 was injected once systemically into the tail vein at a dose of 5×10^8 plaque forming units (PFU)/100 μL 5 days after HCT-116-GFP cells were injected into the spleen. Control mice were injected with 100 μL PBS in an identical manner ($n = 9$ mice per group). Six weeks after tumor cell inoculation (5 weeks after treatment), fluorescence imaging was done using an Olympus OV100 Imaging System. GFP fluorescent intensity of the liver metastases and the number of lung metastases were determined. To obtain GFP intensity, exposure conditions were maintained constant at 30 ms to keep the data comparable. GFP intensity was quantified and presented in the units of SUM green intensity using Cell software (Olympus-Biosystems). The experimental data are presented as mean ± SD. Comparison of the GFP intensity and the number of lung metastases between the treatment and control groups were analyzed using a two-tailed Student's t test.

The antitumor efficacy of i.v. administration of OBP-301 was also assessed in an orthotopic liver tumor model of HCC. OBP-301 was i.v. injected biweekly (5×10^8 PFU/2 weeks for 6 weeks) starting from 2 weeks after Hep3B-GFP cells were injected into the liver. Control mice were injected with 100 μL PBS in an identical manner ($n = 9$ mice per group). All animals were examined 8 weeks after cancer cell inoculation (2 weeks after last treatment). Development of tumor growth and response to OBP-301 treatment were evaluated by the fluorescent area of the liver tumor calculated by Cell software using GFP images obtained with the Olympus OV100. The experimental data are presented as

mean ± SD. Comparison of the tumor area between the treatment and control groups was analyzed using a two-tailed Student's *t* test.

Viral GFP Labeling of Tumors

To assess the tumor detection ability of OBP-401 for metastatic liver tumors, a liver metastasis model of unlabeled HCT-116 cells was used. OBP-401 was injected i.v. or intrasplenically at a dose of 1×10^8 PFU/mouse. Animals were examined at laparotomy by fluorescence imaging with the OV100 5 days after OBP-401 was administered. Some mice had a second-look observation 1 week after the first open examination.

To assess the tumor detection ability of OBP-401 in the orthotopic liver tumor model, unlabeled Hep3B cells were

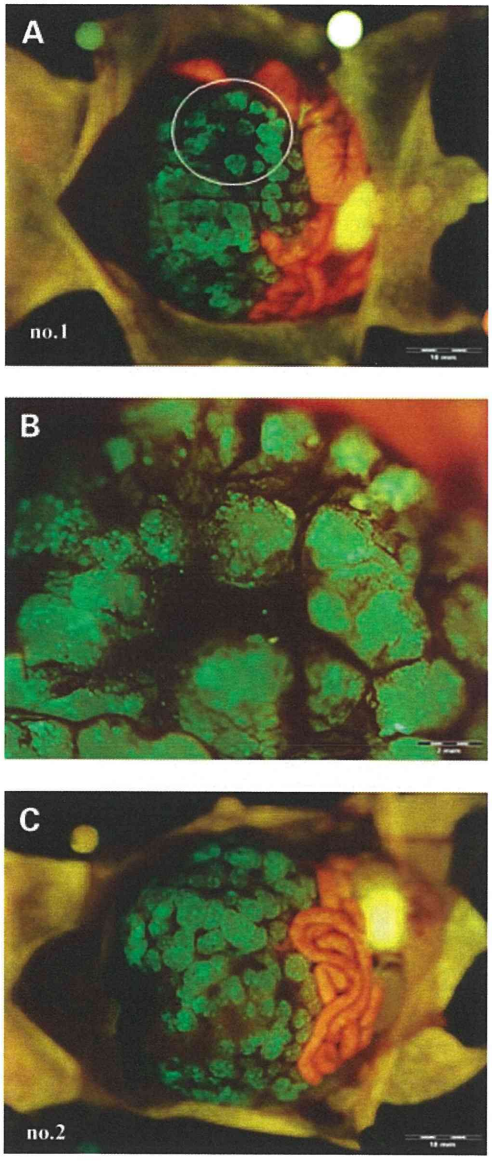

Figure 3. Portal venous delivery of OBP-401 selectively labeled multiple colon cancer liver metastases. **A,** gross appearance of the abdominal cavity (mouse no. 1). Five days after splenic injection of OBP-401, HCT-116 liver metastases were visualized by GFP fluorescence. **B,** higher magnification of the liver surface indicated by the *white circle* in **A**. **C,** liver metastases were visualized by GFP fluorescence in mouse no. 2.

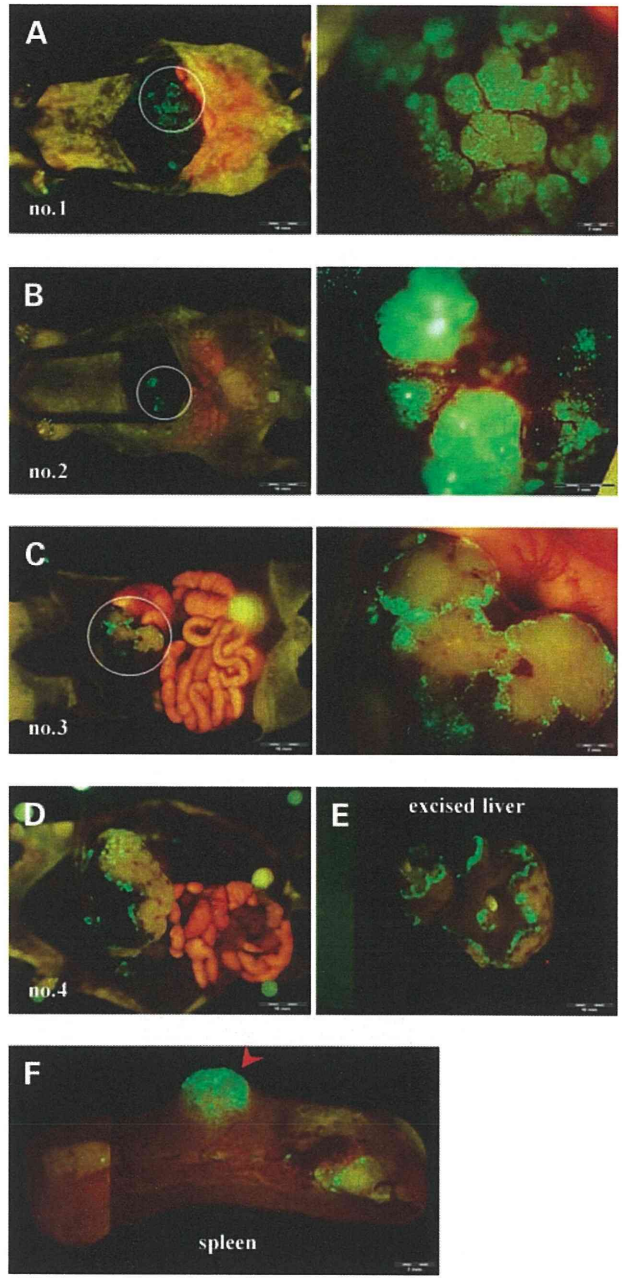

Figure 4. Selective GFP labeling of multiple liver metastases of human colon cancer by i.v. injection of OBP-401. **A** to **C,** 5 d after i.v. injection with OBP-401, HCT-116 liver metastases were visualized by GFP fluorescence (mouse nos. 1-3; *left*). Higher magnification of the liver metastasis indicated by a white circle (*right*). **D,** gross appearance of the abdominal cavity (mouse no. 4). **E,** macroscopic appearance of excised liver in mouse no. 4. The margin of the liver metastasis was visualized by GFP fluorescence. **F,** macroscopic appearance of spleen. Tumor development in the spleen was also visualized by GFP fluorescence 5 d after OBP-401 treatment (*red arrow*).

used. OBP-401 was injected systemically into the tail vein at a dose of 1×10^8 PFU/mouse 2 weeks after tumor cell inoculation. Animals were examined at laparotomy by fluorescence imaging with the OV100 5 days after OBP-401 was administered. Some mice had a second-look observation 4 weeks after i.v. injection of OBP-401.

Fluorescence Optical Imaging and Processing

The Olympus OV100 Imaging System containing an MT-20 light source was used. High-resolution images are captured directly on a PC (Fujitsu Siemens), and images are analyzed with the use of Cell software (Olympus-Biosystems).

Results and Discussion

Liver Metastasis Model of Human Colon Cancer

Intrasplenic inoculation of nude mice with unlabeled HCT-116 or HCT-116-GFP human colon cancer cells led to multiple experimental metastases in the liver within 14 days. With HCT-116-GFP, spleen tumors and lung metastasis could also be observed by fluorescence imaging at 6 weeks after cancer cell implantation.

Orthotopic Liver Tumor Model of HCC

When unlabeled Hep3B or Hep3B-GFP human HCC cells were subserosally injected into the liver of nude mice (Fig. 1A), a small tumor mass (~2 mm) was often observed on the liver surface by 2 weeks after cancer cell inoculation. Hep3B liver tumors usually grew only in the injected lobe and rarely spread to other lobes (Fig. 1B). These tumors showed abundant tumor blood vessels, indicating a rich blood supply for the tumor, which reflects HCC in human patients (Fig. 1C).

Unlabeled HepG2 cells were also inoculated in the spleen of nude mice with the same technique used in the experimental colorectal liver metastasis model. Two weeks after tumor cell inoculation, multiple HepG2 tumors were observed on the liver surface.

Inhibition of Experimental Colon Cancer Metastasis by OBP-301

OBP-301 was i.v. injected at a dose of 5×10^8 PFU/mouse 5 days after HCT-116-GFP inoculation in the spleen. At 6 weeks after HCT-116-GFP colon cancer cell inoculation, 100% of the control animals developed liver tumors, and tumors in the spleen developed in 40% of control animals. Treatment with OBP-301 caused a significant inhibition in liver metastasis growth ($P < 0.05$; Fig. 2A and D). Additionally, OBP-301–treated animals showed a reduced number of lung metastases colonies compared with controls ($P < 0.05$; Fig. 2B and E). These results show that systemic dosing of OBP-301 has significant antitumor activity against experimental colon cancer liver metastasis. In contrast to the experimental liver metastasis, OBP-301 did not have an apparent effect on the spleen tumors. The lack of effect of OBP-301 on the spleen tumors may be because of their very small size, which made differences difficult to discern.

Inhibition of Orthotopic HCC by OBP-301

To evaluate the antitumor efficacy of OBP-301 on HCC tumors, the orthotopic liver tumor model of Hep3B-GFP was used.

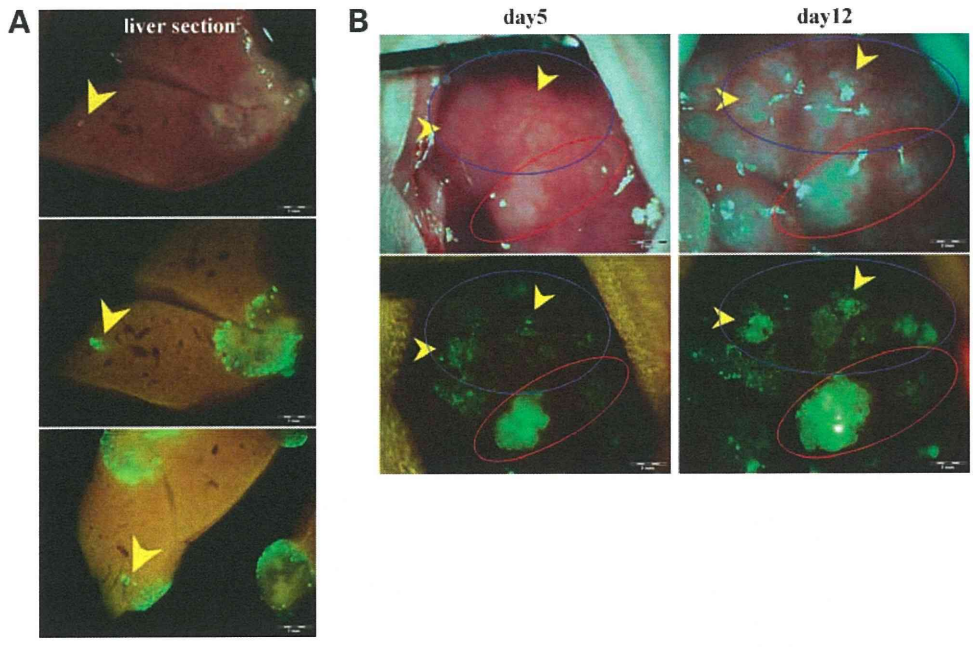

Figure 5. Early metastatic liver tumors not otherwise clearly visible could be visualized after i.v. injection of OBP-401. **A,** cross-sections of liver. GFP expression was mainly located at the periphery of the liver metastases. Tiny metastatic foci not otherwise clearly visible were visualized by GFP fluorescence after i.v. injection of OBP-401 (*yellow arrow*). **B,** 5 d after i.v. injection of OBP-401, HCT-116 liver metastases were visualized by GFP fluorescence (*red circle*). There were areas in the liver, which had GFP expression but seemed to be tumor-free in bright light (*blue circle*). Seven days later, metastases could be visualized by bright light as well as GFP fluorescence (*yellow arrows*), showing the power of OBP-401 to label very early, otherwise invisible metastases with GFP.

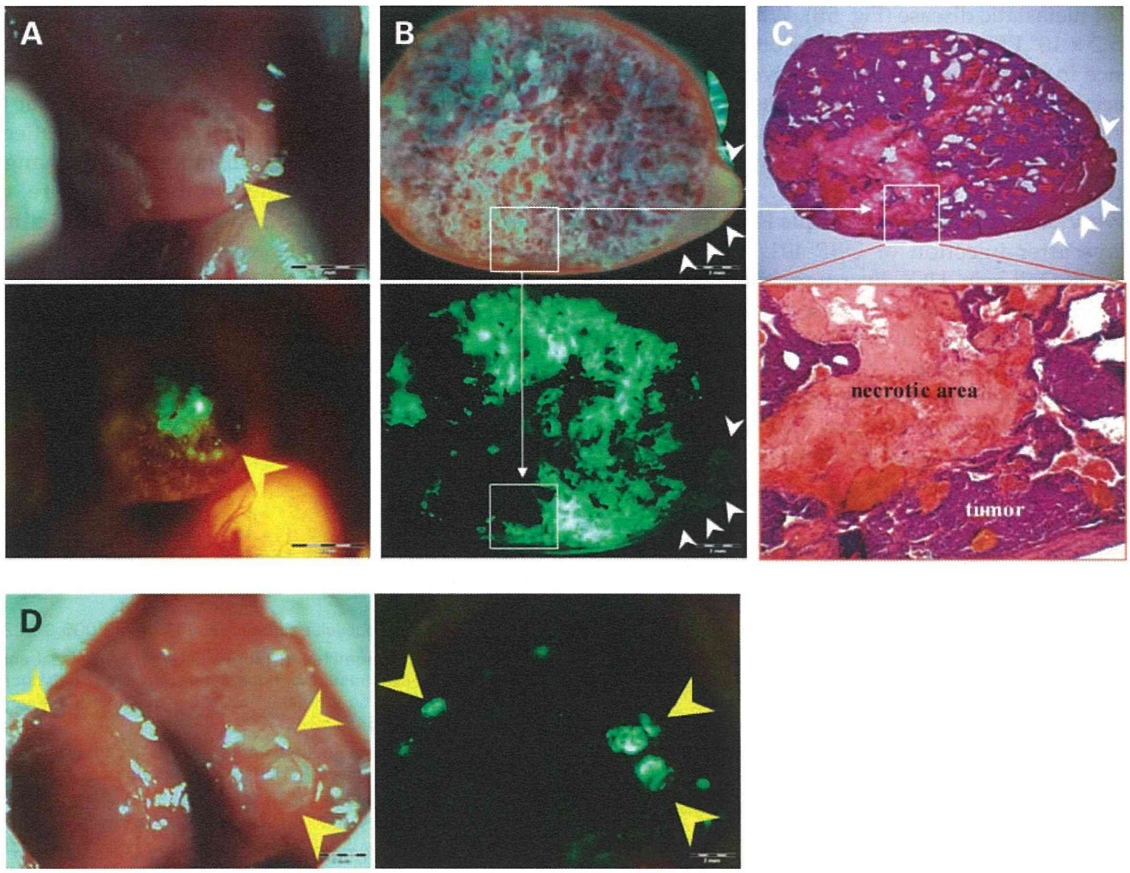

Figure 6. Selective visualization of orthotopic HCC tumors by i.v. injection of OBP-401. **A,** 5 d after systemic administration of OBP-401, orthotopic Hep3B HCC was visualized by GFP fluorescence (*yellow arrow*). *Top,* bright-field observation; *bottom,* fluorescence detection. **B,** cross-section of liver tumor 4 wk after i.v. injection of OBP-401. GFP expression was selectively detected in the tumor. *White arrow* indicates normal liver tissue. *Top,* bright-field observation; *bottom,* fluorescence detection. **C,** H&E section of Hep3B liver tumor of **B**. *Top,* magnification, ×10; *bottom,* detail of the boxed region. Magnification, ×40. Boxes refer to corresponding regions in **B** and **C** with high magnification in **B** and **C** (*bottom*). **D,** orthotopic HepG2 HCC tumors (*yellow arrows*) were visualized by GFP fluorescence (*yellow arrows*) 4 wk after i.v. injection of OBP-401.

The colorectal liver metastasis model was made by delivering cells into the portal vein as described above, whereas the orthotopic HCC model was made by injecting cells directly into the hepatic parenchyma, where at the early stage of tumor development most cells were thought to locate outside of the blood vessels. Thus, i.v. injected OBP-301 could target cancer cells more effectively in the colorectal liver metastasis model than in the HCC model. In the HCC model, therefore, we increased the number of injections of OBP-301, which was administered biweekly (5×10^8 PFU/2 weeks i.v. for 6 weeks) starting 2 weeks after tumor cell inoculation. Treatment of OBP-301 caused a significant inhibition in liver tumor growth ($P < 0.01$; Fig. 1D and E). These results show that systemic dosing of OBP-301 has significant antitumor activity against Hep3B-GFP human HCC tumors.

Selective Visualization of Colorectal Liver Metastases by OBP-401 Delivery of the GFP Gene

To assess the tumor detection ability of OBP-401 for colorectal liver metastases, OBP-401 was administrated to mice by portal venous delivery or systemic delivery using the tail vein.

Animals with HCT-116 experimental liver metastases were intrasplenically injected with OBP-401 (1×10^8 PFU/mouse) 12 days after tumor cell inoculation. The spleen was used to access the portal venous circulation. Five days after injection of OBP-401, the liver metastases could be visualized by GFP fluorescence. Representative mice are shown in Fig. 3. Cross-sections of the liver showed that GFP fluorescence occurred mainly at the periphery of the metastatic liver nodules (data not shown). Liver metastases in mice given 1×10^7 PFU of OBP-401 were not visualized efficiently by GFP expression (data not shown), indicating dose response.

HCT-116 liver metastases could also be visualized by GFP fluorescence after i.v. injection of OBP-401 (1×10^8 PFU/mouse; Fig. 4). Cross-sections of the liver also showed tiny metastatic foci visualized by GFP fluorescence (Fig. 5A). Moreover, a second-look observation done 1 week after the first laparotomy showed that early metastatic liver tumors, not clearly visible under bright light, had been visualized with GFP fluorescence after i.v. injection of OBP-401 at as early as day 5, indicating the possibility of early

detection of metastatic disease (Fig. 5B). When injected with more than 2×10^8 PFU of OBP-401, mice often showed GFP fluorescence in normal tissues such as liver, lung, spleen, and thoracic duct (data not shown). Theses results suggest that colorectal liver metastases can be visualized by GFP fluorescence both by portal venous and i.v. administration of OBP-401.

Selective Visualization of Orthotopic HCC by OBP-401

Five days after injection of OBP-401 (1×10^8 PFU/mouse) into the tail vein, HCC liver tumors were visualized by GFP fluorescence (Fig. 6A). Cross-sections of the liver at 4 weeks after i.v. injection of OBP-401 showed that GFP expression was in the cancer cells and not in normal cells (Fig. 6B and C). Small liver tumor nodules were also visualized by GFP fluorescence after i.v. OBP-401 administration (Fig. 6D). Thus, we showed that HCC liver tumors could be selectively visualized by GFP fluorescence after i.v. injection of OBP-401.

Many studies have shown that the majority of malignant human tumors tested express hTERT. OBP-301 and OBP-401 specifically replicate in tumors due to hTERT expression in tumors (11, 12, 17–19). In previous studies, OBP-301 and OBP-401 were administered locally, such as by intratumoral or intrapleural administration. The present report shows the systemic efficacy of OBP-301 and OBP-401 to selectively replicate in and kill and label primary and metastatic liver tumors after i.v. administration. Closely related virus constructs will be compared with OBP-301 and OBP-401 in the future.

Our laboratory pioneered the use of fluorescent proteins to visualize cancer cells *in vivo*. Cancer cells genetically labeled by fluorescent proteins have increased the possibility and sensitivity to observe progression of cancer cells in live animals (21). To evaluate antitumor efficacy of i.v. administration of OBP-301 against primary and metastatic liver tumors, we used GFP-expressing human cancer cell lines. We showed that i.v. administration of OBP-301 resulted in a significant reduction in experimental liver and pulmonary metastases in a colorectal liver metastases model and effectively inhibited tumor formation and growth in an orthotopic HCC model. OBP-401 has less but still significant cytotoxic effects compared with OBP-301 (22). In fact, a significant inhibition of tumor growth by intratumoral injection of OBP-401 was confirmed *in vivo* in our previous study (20). However, OBP-401 at the tumor-selective labeling dose used in this i.v. injection study could not inhibit tumor growth effectively.

The imaging strategy using OBP-401 has a potential of being available in humans as a navigation system in the surgical treatment of malignancy. During surgery, tumors that would be difficult to detect by direct visual detection could be positively identified with GFP fluorescence using a handheld excitation light and appropriate filter goggles as we have shown previously in mice (23–25). Employment of a fluorescence surgical microscope would enable visualization of the GFP-expressing microscopic leading edge of the tumor and allow accurate resection with sufficient margins.

As for toxicity of OBP-301 and OBP-401, only when injected with 5×10^8 PFU OBP-301 for the first time, a few mice showed lethargy but fully recovered within 1 h. None of the mice treated with OBP-301 or OBP-401 at the doses used in this study showed significant adverse effects during the observation period or histopathologic changes in the liver at the time of sacrifice. In the near future, the safety of OBP-301 will be confirmed in a phase I clinical trial, which is currently under way (26).

Our studies suggest the clinical potential of OBP-301 and OBP-401.

Disclosure of Potential Conflicts of Interest

No potential conflicts of interest were disclosed.

References

1. Bruix J, Hessheimer AJ, Forner A, Boix L, Vilana R, Llovet JM. New aspects of diagnosis and therapy of hepatocellular carcinoma. Oncogene 2006;25:3848–56.
2. Okuda K. Hepatocellular carcinoma. J Hepatol 2000;32:225–37.
3. Takayasu K, Muramatsu Y, Moriyama N, et al. Clinical and radiologic assessments of the results of hepatectomy for small hepatocellular carcinoma and therapeutic arterial embolization for postoperative recurrence. Cancer 1989;64:1848–52.
4. Koshariya M, Jagad RB, Kawamoto J, et al. An update and our experience with metastatic liver disease. Hepato-gastroenterology 2007;54:2232–9.
5. Kavolius J, Fong Y, Blumgart LH. Surgical resection of metastatic liver tumors. Surg Oncol Clin N Am 1996;5:337–52.
6. Chouillard E, Cherqui D, Tayar C, Brunetti F, Fagniez PL. Anatomical bi- and trisegmentectomies as alternatives to extensive liver resections. Ann Surg 2003;238:29–34.
7. Jiao LR, Hansen PD, Havlik R, Mitry RR, Pignatelli M, Habib N. Clinical short-term results of radiofrequency ablation in primary and secondary liver tumors. Am J Surg 1999;177:303–6.
8. Khatri VP, Petrelli NJ, Belghiti J. Extending the frontiers of surgical therapy for hepatic colorectal metastases: is there a limit? J Clin Oncol 2005; 23:8490–9.
9. Adam R. Chemotherapy and surgery: new perspectives on the treatment of unresectable liver metastases. Ann Oncol 2003;14 Suppl 2:ii13–6.
10. Bismuth H, Adam R, Lévi F, et al. Resection of nonresectable liver metastases from colorectal cancer after neoadjuvant chemotherapy. Ann Surg 1996;224:509–20, discussion 520–2.
11. Kawashima T, Kagawa S, Kobayashi N, et al. Telomerase-specific replication-selective virotherapy for human cancer. Clin Cancer Res 2004;10: 285–92.
12. Taki M, Kagawa S, Nishizaki M, et al. Enhanced oncolysis by a tropism-modified telomerase-specific replication-selective adenoviral agent OBP-405 ('telomelysin-RGD'). Oncogene 2005;24:3130–40.
13. Umeoka T, Kawashima T, Kagawa S, et al. Visualization of intrathoracically disseminated solid tumors in mice with optical imaging by telomerase-specific amplification of a transferred green fluorescent protein gene. Cancer Res 2004;64:6259–65.
14. Hashimoto Y, Watanabe Y, Shirakiya Y, et al. Establishment of biological and pharmacokinetic assays of telomerase-specific replication-selective adenovirus. Cancer Sci 2008;99:385–90.
15. Kishimoto H, Kojima T, Watanabe Y, et al. *In vivo* imaging of lymph node metastasis with telomerase-specific replication-selective adenovirus. Nat Med 2006;12:1213–9.
16. Takakura M, Kyo S, Kanaya T, et al. Cloning of human telomerase catalytic subunit (hTERT) gene promoter and identification of proximal core promoter sequences essential for transcriptional activation in immortalized and cancer cells. Cancer Res 1999;59:551–7.
17. Watanabe T, Hioki M, Fujiwara T, et al. Histone deacetylase inhibitor FR901228 enhances the antitumor effect of telomerase-specific

replication-selective adenoviral agent OBP-301 in human lung cancer cells. Exp Cell Res 2006;312:256–65.

18. Hioki M, Kagawa S, Fujiwara T, et al. Combination of oncolytic adenovirotherapy and Bax gene therapy in human cancer xenografted models. Potential merits and hurdles for combination therapy. Int J Cancer 2008;122:2628–33.

19. Huang P, Watanabe M, Kaku H, et al. Direct and distant antitumor effects of a telomerase-selective oncolytic adenoviral agent, OBP-301, in a mouse prostate cancer model. Cancer Gene Ther 2008;15:315–22.

20. Fujiwara T, Kagawa S, Kishimoto H, et al. Enhanced antitumor efficacy of telomerase-selective oncolytic adenoviral agent OBP-401 with docetaxel: preclinical evaluation of chemovirotherapy. Int J Cancer 2006;119:432–40.

21. Hoffman RM. The multiple uses of fluorescent proteins to visualize cancer *in vivo*. Nat Rev Cancer 2005;5:796–806.

22. Kyo S, Takakura M, Fujiwara T, Inoue M. Understanding and exploiting hTERT promoter regulation for diagnosis and treatment of human cancers. Cancer Sci 2008;99:1528–38.

23. Yang M, Luiken G, Baranov E, Hoffman RM. Facile whole-body imaging of internal fluorescent tumors in mice with an LED flashlight. Biotechniques 2005;39:170–2.

24. Kishimoto H, Zhao M, Hayashi K, et al. *In vivo* internal tumor illumination by telomerase-dependent adenoviral GFP for precise surgical navigation. Proc Natl Acad Sci U S A 2009;106:14514–7.

25. Jasni BR. Green surgery. Science 2009;325:1321.

26. Fujiwara T, Tanaka N, Numunaitis JJ, et al. Phase I trial of intratumoral administration of OBP-301, a novel telomerase-specific oncolytic virus, in patients with advanced solid cancer. Evaluation of biodistribution and immune response. J Clin Oncol 2008;26:3572.